Physics of the Earth and Planetary Interiors, 41 (1985) 34–57
Elsevier Science Publishers B.V., Amsterdam – Printed in The Netherlands

Numerical models on the influence of partial melt on elastic, anelastic and electric properties of rocks. Part I: elasticity and anelasticity

Harro Schmeling *

Institut fuer Meteorologie and Geophysik, Feldbergstrasse 47, 6000 Frankfurt/Main (F.R.G.)

(Received January 15, 1985; revision accepted February 18, 1985)

Schmeling, H., 1985. Numerical models on the influence of partial melt on elastic, anelastic and electric properties of rocks. Part I: elasticity and anelasticity. Phys. Earth Planet. Inter., 41: 34–57.

With the aim of a simultaneous interpretation of elastic, anelastic and electric in situ data from the asthenosphere a comprehensive set of numerical models is developed for partial melt in different geometrical configurations. For the elastic and anelastic modulus use is made throughout of the melt squirt mechanism. Frequency dependence is not treated in detail but estimated from the limiting cases of the relaxed and unrelaxed modulus. This has the advantage that quantitative values of viscocity and flow path dimensions are not required. In the models melt can be assumed to occur in the form of tubes, films, and triaxial ellipsoidal inclusions of arbitrary aspect ratio. The conditions in which the solutions for triaxial ellipsoidal inclusions can be approximated by simpler ones for spheroidal inclusions are discussed. It is then shown up to which aspect ratio a published model on melt films is applicable. The problem of interconnection of inclusions is treated with a statistical numerical approach. It is found that a reduced degree of interconnection may have a significant influence on anelastic relaxation at melt fractions corresponding to a moderate modulus decrease. A useful representation of the anelastic melt models is introduced by plotting the relaxation strength against the effective modulus, both of which depend on the state of melting. Such diagrams allow a clear distinction between the different melt geometries and may be used for the interpretation of observed data. Finally, different melt geometries are superimposed and it is found that under certain conditions bulk dissipation may reach the order of that for shear.

1. Introduction

Seismological and magnetotelluric investigations have shown that mantle regions of low seismic velocities can generally be correlated with those of high seismic absorption and high electrical conductivity. In such zones the geotherm may approach or exceed the solidus temperature. The melt fraction, geometry, and degree of interconnection strongly influences the seismic velocities, the seismic absorption, and the electrical conductivity, but in different manners.

A number of theoretical investigations focus on the relationship between the seismic properties and partial melt, assuming different idealized melt geometries (Walsh, 1969; O'Connell and Budiansky, 1977; Mavko, 1980). Other workers have discussed the dependence of the electrical conductivity on the amount of partial melt (Waff, 1974; Shankland and Waff, 1974; Haak, 1980). In part I and II of the present paper a numerical set of melt models is developed in which the idealized melt geometries, the degree of interconnection, and the melt fraction are varied systematically. The effect of partially molten material on both seismic and electric properties is studied. These seismic and electric models are combined in a model set, which is applicable to in situ data. In additional papers

* Present address: University of Uppsala, Institute of Geology, Department of Mineralogy and Petrology, Box 555, S-75122 Uppsala, Sweden.

0031-9201/85/$03.30

(Schmeling, 1984, 1985, and in prep.(a)) the melt models are applied to data of the oceanic asthenosphere and the anomalous mantle below Iceland. For more details on the methods used reference is made to Schmeling (1983).

2. The occurrence of partial melt

It is widely accepted that the undepleted upper mantle has a pyrolitic composition (Ringwood, 1962a,b, 1975). Besides that of possible variations in composition the water content strongly influences the solidus temperature. In upper mantle conditions small amounts of water ($< 0.4\%$) may reduce the solidus temperature by several hundred degrees (Green and Lieberman, 1976). A compilation of several melting curves of pyrolite at different pressures and water contents is shown in Fig. 1.

The geometrical distribution and the connectiveness of the melt in a partially molten polycrystalline rock is determined by three factors: (1) the melt fraction; (2) the location of melt; and (3) the minimum total free energy of the solid–solid and the solid–liquid interfaces. The latter condition

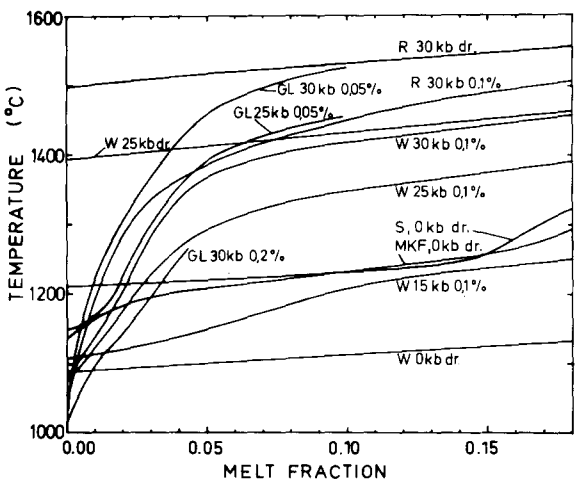

Fig. 1. Melting curves of pyrolite and spinel lherzolite at different pressures and water concentrations (values in %, dr.: dry). W: Wyllie (1971); R: Ringwood (1975); GL: Green and Liebermann (1976); MKF: Murase et al. (1977), S: Scarfe et al. (1972).

determines the dihedral angle, ϕ (which is defined according to Fig. 2a) and, furthermore, it implies that the curvature of the solid–liquid interface should have a constant minimum value. Possible melt distributions for different dihedral angles are shown in Fig. 2 (after Stocker and Gordon, 1975 and Kingery et al., 1976). If $\phi = 0°$ the melt wets all grain faces, if $0° < \phi < 60°$ the melt situated at grain edges or corners will form an interconnected system of tubes, and if $\phi > 60°$ the melt will be concentrated in pockets at grain corners. Bulau et al. (1979) argued that even when $\phi = 0°$ the melt should occur only within tubes along grain edges similar to Fig. 2c but with more pronounced cusps. However, this would imply that a considerable amount of the dry grain boundaries would have a higher level of surface energy as compared to the case of complete wetting. If melt occurs within grains, it is expected to have a spherical geometry as a consequence of minimum surface energy. Inclusions occurring at grain faces but not reaching the grain edges will have a disc or spherical shape (see block digrams in Fig. 2).

When $\phi > 60°$ it is obvious that the possibility of interconnection of the melt inclusions is dependent on the grain geometry and the amount of melt. Bulau et al. (1979) determined the critical melt fraction leading to an interconnected system of melt pockets as a function of the dihedral angle. They found a steady increase from 0 to 30% critical melt fraction for angles increasing from 60 to 180°.

Most melting experiments find that the melt occurs in films wetting the grain faces (Arzi, 1972, 1978a,b; Mehnert et al., 1973; Buesch et al., 1974; Arndt, 1977; Van der Molen and Paterson, 1979) although compact melt pockets have also been observed in dunite (Berckhemer et al., 1982a,b). Waff and Bulau (1979) carried out melting experiments with mechanical mixtures of dunite and basalt powders and approached the textural equilibrium. They found the melt occurring within intergranular tubes with a mean dihedral angle of 47°, the grain faces appeared to be dry (Cooper and Kohlstedt, 1982). A completely connected melt system was found for a melt fraction of 1–2% in tubes (Waff and Bulau, 1979), but 5–10% were needed in the case of films (Mehnert et al., 1973;

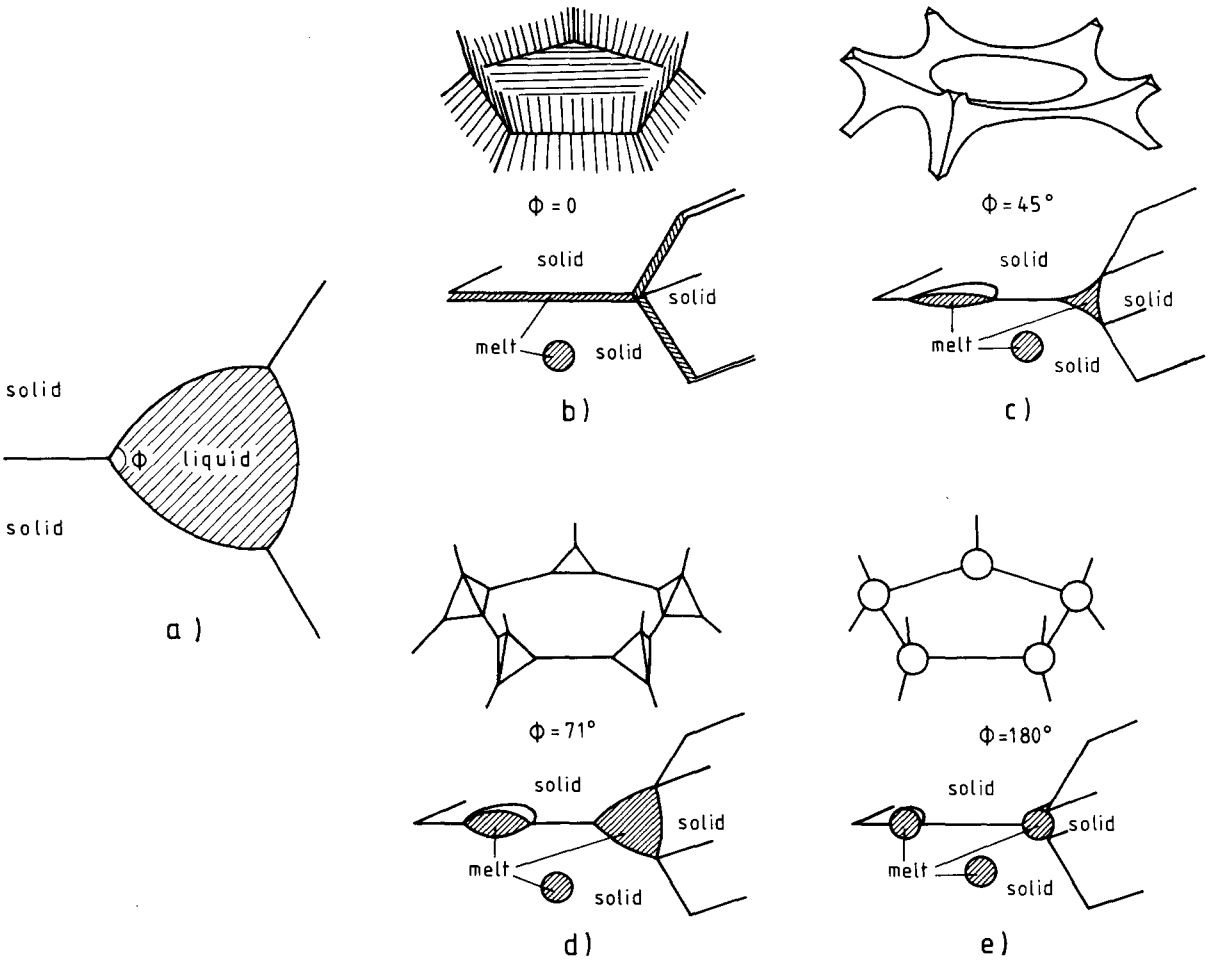

Fig. 2. (a) Illustration of the definition of the dihedral ange ϕ. (b–e) Possible geometries of the melt phase in a partially molten rock: films (b), tubes (c), and melt pockets (d and e). The hatched areas in the block diagrams (lower part of each Figure) also show possible melt geometries depending on the location of the melt within grains, at grain faces, or at grain edges.

Arndt, 1977). Arzi (1974, 1978a) and Van der Molen and Paterson (1979) observed an increase of dry grain faces if the melt fraction decreases. The specimens of peridotite and dunite used in the experiments by Berckhemer et al. (1979, 1982a) also showed melt films at some, but not all grain faces (B. Aitken, personal communication, 1981). Padovani (1977) observed evidence for both connected and unconnected melt in xenoliths at Kilbourne Hole, New Mexico, which originated from the lower crust and partially melted during ascent.

Assessing all the arguments and observations mentioned above it appears reasonable to consider the whole variety of possible melt geometries and a variable degree of interconnection when formulating melt models describing the elasticity, anelasticity, and electrical conductivity of partially molten rocks.

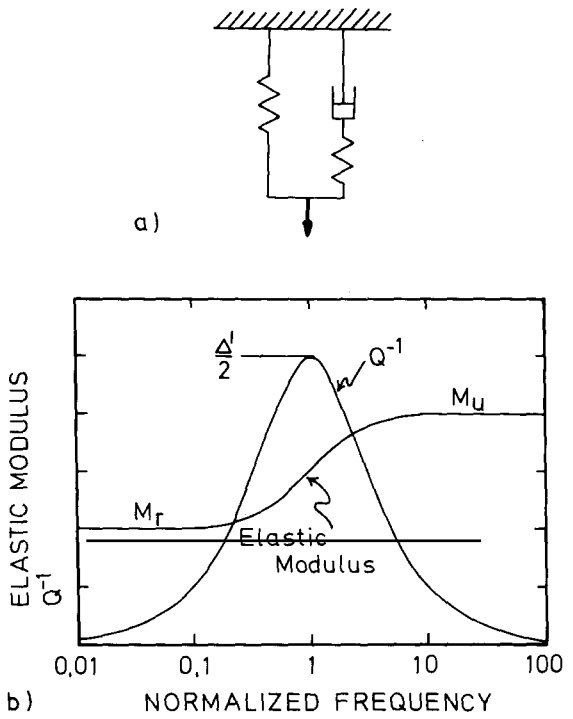

Fig. 3. Standard linear solid. (a). Symbolic representation. (b). Corresponding elastic modulus and internal friction (arbitrary units) as a function of normalized frequency.

3. Basic relations

In a linear viscoelastic body stress and strain can be related by the complex elastic modulus M

$$M = M_1 + iM_2 = |M| \exp(i\psi) \tag{1}$$

M may be any one of the elastic moduli or a linear combination of these. In general M is frequency dependent. The unrelaxed and relaxed moduli M_u and M_r can be defined by the following limits which are real numbers

$$M_u = \lim_{\omega \to \infty} M(\omega)$$
$$M_r = \lim_{\omega \to 0} M(\omega) \tag{2}$$

The absorption factor Q^{-1} can be defined by the complex modulus

$$Q^{-1} = M_2/M_1 = \tan \psi \tag{3}$$

A basic viscoelastic body is the standard linear solid introduced by Zener (1948). It consists of two springs and one damping element (Fig. 3a). The elastic modulus and the corresponding Debye peak of absorption of such a standard linear solid are shown in Fig. 3b as functions of the frequency. A single Debye peak is characterized by a relaxation time τ and the relaxation strength Δ

$$\Delta = \frac{M_u - M_r}{M_r} \tag{4}$$

The amplitude of a Debye peak is given by

$$Q^{-1}_{max} = \Delta'/2 = \frac{M_u - M_r}{2\sqrt{M_u \cdot M_r}} \tag{5}$$

This modified relaxation strength Δ' will be used throughout this paper as an estimate for anelasticity. For small Δ one can write

$$Q^{-1}_{max} \simeq \Delta/2 \tag{6}$$

A real viscoelastic material can be approximated by superimposing different relaxation times. If their normalized distribution is given by $V(\tau)d\tau$, the real and imaginary parts of the modulus can be written (Nowick and Berry, 1972)

$$M_1(\omega) = M_r + (M_u - M_r)\int_0^\infty V \frac{\omega^2\tau^2}{1+\omega^2\tau^2} d\tau \tag{7}$$

$$M_2(\omega) = (M_u - M_r)\int_0^\infty V \frac{\omega\tau}{1+\omega^2\tau^2} d\tau \tag{8}$$

From (8) one can estimate the upper bound for Q^{-1} of an arbitrary distribution V given between τ_1 and τ_2 by applying the mean value theorem for integrals

$$M_2(\omega) = (M_u - M_r)\frac{\omega\tilde{\tau}}{1+\omega^2\tilde{\tau}^2}\int_{\tau_1}^{\tau_2} V d\tau$$
$$= (M_u - M_r)\frac{\omega\tilde{\tau}}{1+\omega^2\tilde{\tau}^2} \leq (M_u - M_r)/2$$

where $(\tau_1 \leq \tilde{\tau}(\omega) \leq \tau_2)$Thus

$$Q^{-1} \leq \Delta/2 \tag{9}$$

for all possible distributions of relaxation processes.

Another useful relation results from the Kramers–Krönig-relation which combines real and imaginary parts of the modulus. After Nowick and Berry (1972, p. 37) the Kramers–Krönig-relation

for M_1 can be written

$$M_1(\omega) = M_r + \frac{2\omega^2}{\pi}\int_0^\infty \frac{M_2(\tilde{\omega})}{\tilde{\omega}}\frac{d\tilde{\omega}}{\omega^2-\tilde{\omega}^2} \qquad (10)$$

From this one obtains

$$M_u = M_r + \frac{2}{\pi}\int_0^\infty M_2(\omega)\,d\ln\omega$$

For small Δ it follows

$$\Delta/2 \simeq \frac{1}{\pi}\int_0^\infty Q^{-1}(\tilde{\omega})\,d\ln\tilde{\omega} \qquad (11)$$

Thus the half relaxation strength can be approximated by the area of the Q^{-1}-spectrum plotted versus $\ln\omega$ and divided by π. (11) can be used to estimate Q^{-1} for given relaxation strengths and certain relaxation spectra. For instance, assuming a constant Q band model over the range $1/\tau_2 \ll \omega \ll 1/\tau_1$, Q is related to Δ (cf. Mavko, 1980) by

$$Q^{-1} \simeq \Delta/2\,\frac{1.36}{\log_{10}\tau_2 - \log_{10}\tau_1} \qquad (12)$$

which varies only weakly with the width of the band.

In the model set presented below the relaxed and unrelaxed moduli and the relaxation strength are considered for a partially molten material. The explicit frequency dependence of the moduli and Q was not treated in detail. Equations 7–12, together with assumptions about relaxation spectra, can be used to estimate the behaviour of Q with frequency. As an advantage of this simplified approach a detailed knowledge of the melt viscosity is not required.

4. Previous work

This section reviews earlier models of elasticity and anelasticity which include relaxed and unrelaxed states as well as frequency dependent absorption models of general solid–fluid systems (see also Watt et al., 1976; Mavko et al., 1979).

4.1. Elasticity moduli

Early estimates of bounds of moduli for composite materials (Voigt, 1928; Reuss, 1929) assumed highly anisotropic materials. Hashin and Shtrikman (1963) gave bounds on the elastic constants of an isotropic material (subsequently denoted as HS-bounds). They showed, that without knowledge of the geometry of the components, the HS-bound of the bulk modulus is the best possible. The lower HS-bound of the shear modulus of a solid–fluid system is of no use since it is zero. A useful alternative is to specify the geometry of the phases. If the fluid phase occurs in widely separated inclusions, the elastic interactions between inclusions can be neglected. Under this assumption Eshelby (1957) and Hashin (1959) derived expressions for the bulk and shear moduli of a material containing spherical inclusions. Surprisingly, the moduli lie above the HS-bounds and approach these only at small fluid concentrations. Since this discrepancy is due to the neglect of elastic interactions it can give an idea about the validity of the non-interaction assumption.

Eshelby (1957) investigated the elastic field of an ellipsoidal elastic or fluid inclusion embedded in a homogeneous elastic medium under external stress. Using Eshelby's (1957) results Wu (1966) derived analytical expressions for the effective moduli for the case of spheroidal ($a = b \neq c$), penny shaped ($a = b \gg c$), and needle shaped ($a \gg b = c$) inclusions, where a,b,c are the three half axes of the ellipsoidal inclusion. For the case of soft penny shaped inclusions Wu's formulae are no more applicable. Walsh (1969) modified them for fluid inclusions with a small but finite aspect ratio $\alpha(= c/a)$. In contrast to Wu's moduli Walsh's results are only valid for the case of non-interaction between the inclusions, which leads to difficulties at fluid concentrations of the same order as aspect ratios (Schmeling, in prep.(b)).

To take into account the interaction between inclusions and thus allow for higher concentrations the most successful approach so far is the "self consistent scheme" (Budiansky, 1965; Hill, 1965), subsequently abbreviated as "SCS". Rather than considering explicitly the elastic interactions between densely distributed inclusions one approximates the elastic field around a particular inclusion by embedding it in an infinite homogeneous medium with the mean effective moduli to be determined. This leads to an implicit system of

coupled equations for the effective moduli. With this approach the effective moduli of a solid containing spherical inclusions lie well between the HS-bounds.

A very comprehensive study of the elasticity of a material containing dry cracks or thin fluid films was carried out by O'Connell and Budiansky (1974, 1977) and Budiansky and O'Connell (1976). They approximated the cracks respective films by flat ellipsoidal inclusions with the axes a, $b \gg c$. The SCS was applied. The parameter determining the elasticity was the crack density, defined as

$$\epsilon = 2\frac{N}{\pi}\frac{A^2}{P} \tag{13}$$

where N is the number of cracks per volume, A is the area and P is the perimeter of a crack. In the case of circular cracks with the radius a' (13) reduces to

$$\epsilon = Na'^3 \tag{14}$$

This crack density is related to the porosity (or fluid fraction) β and the aspect ratio α $(= c/a')$ by

$$\beta = 4\pi\alpha\epsilon/3 \tag{15}$$

O'Connell and Budiansky (1974) showed that the elastic moduli of a material containing elliptical cracks with $a \neq b \gg c$ are nearly equal to those of circular cracks $(a' = b' \gg c)$ as long as the crack densities defined by (13) and (14) are the same. Keeping β and the small axis c constant, the radius of the circular cracks a' is related to A and P of the elliptical cracks

$$a' = 2A/P \tag{16}$$

O'Connell and Budiansky (1977) introduced the crack density in a form allowing for distributed inclusion shapes. If $V(\alpha)$ is the normalized distribution of aspect ratios, the aspect ratio α and the quantity D in O'Connell and Budiansky's equations for both the unrelaxed and relaxed moduli (or in eq. B7 in our Appendix B) have to be replaced by

$$\alpha' = \int_0^\infty V(\alpha)\alpha \mathrm{d}\alpha \tag{17}$$

$$D' = \int_0^\infty DV(\alpha)\mathrm{d}\alpha$$

For the relaxed shear modulus an arbitrary distribution of α can thus be represented by exactly one aspect ratio α' (because $D = 1$, see Appendix B). For unrelaxed moduli this is only approximately the case as long as $\alpha \ll K_f/K$, where K, K_f are the bulk moduli of the effective material and of the fluid, respectively.

The inclusion geometries mentioned so far have always been convex so that for cracks the opposite faces are decoupled over their entire area regardless how small the aspect ratio is. However, microscopic investigations of cracked rocks show that many (or most) of the cracks are irregular and the faces have local point contact (Walsh and Grosenbaugh, 1979). Such contacts increase in area with lithostatic pressure if the cracks are dry or filled with a compressible fluid. Thus, when using models of ellipsoidal cracks caution must be taken if small aspect ratios are assumed because the "effective" aspect ratio may be larger due to the contacts at the faces. Theoretical models for the compressibility in the case of non-ellipsoidal cracks were developed by Mavko and Nur (1978) and Walsh and Grosenbaugh (1979). However, similar models for the shear modulus are missing.

Mavko (1980) determined the effective moduli for the fluid (i.e., melt) distributed in form of tubes along grain edges (Fig. 2c). He varied the shape of the cross section of the tubes by a parameter κ (Fig. 4) and used the SCS to determine the dry and saturated shear moduli and the dry bulk modulus. However, for the determination of the saturated bulk modulus he used Gassmann's (1951) relation together with the self consistent dry modulus. This inconsistency is discussed in Appendix A.

The effect of applying the SCS can be demon-

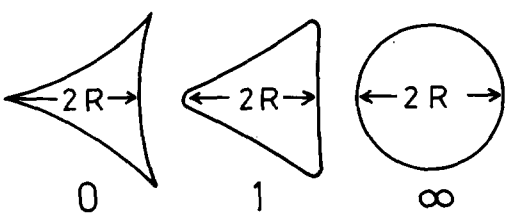

Fig. 4. Shapes of cross-sections of the tube model after Mavko (1980) depending on the parameter κ. (From: Mavko, 1980.)

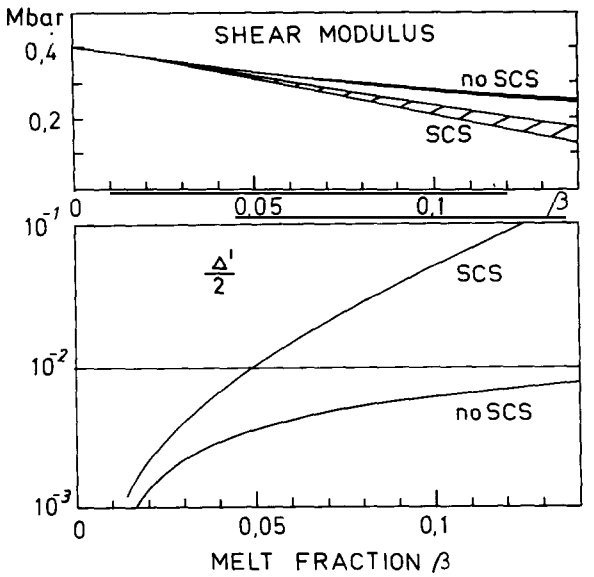

Fig. 5. Shear modulus (upper diagram) and half relaxation strength $\Delta'/2$ (lower diagram) for the tube model ($\kappa = 0$) of Mavko (1980), calculated with and without applying the SCS. The lower (upper) curves of the shear modulus represent the relaxed (unrelaxed) state.

strated using Mavko's (1980) model. In Fig. 5 the shear modulus (top) and maximum shear absorption ($\simeq$ half relaxation strength) (bottom) are shown with and without applying the SCS as a function of melt fraction β. Above 5% melt the moduli begin to diverge slightly. However, the absorption with the SCS shows a striking difference compared to that without the SCS even at melt fractions as low as 5%. This raises the question on the reliability of the SCS for the determination of relaxation strength relative to that of the corresponding moduli.

4.2. Relaxation models

In the following part of this section absorption mechanisms in a solid–liquid system are discussed. Biot (1956a,b) developed a theory describing seismic wave propagation and absorption in a fluid saturated porous medium. Biot's theory considers a regional flow of the fluid with respect to the solid as a result of inertia and a pressure gradient along the seismic wave length. This mechanism appears insufficient to account for seismic absorption in a partial melt (Schmeling, 1983). On the other hand, due to microscopic heterogeneities such as variable geometries and orientations of pores a locally inhomogeneous flow field may become important, which is not accounted for in Biot's approach. In particular, elastic energy may be dissipated either by viscous shear between opposed boundary faces of fluid films, or flow driven by pressure gradients within or between pores.

4.2.1. Viscous shear

Walsh (1968, 1969) calculated the viscous shear relaxation of a material containing penny shaped randomly distributed and oriented fluid inclusions. He found that such a material behaves like a standard linear solid with a characteristic relaxation frequency depending on the aspect ratio and the fluid viscosity. Walsh also estimated the relaxation strength, however, the solution is only valid for widely dispersed inclusions and it cannot be applied to the case of complete grain boundary relaxation. O'Connell and Budiansky (1977) carried out a viscoelastic analysis of viscous shear relaxation in fluid filled cracks. Owing to the SCS used the effective complex shear and bulk moduli become coupled. Thus, the model material loses the property of a standard linear solid. Since eqs. 4–12 are based on the standard linear solid, the deviation due to the SCS is assessed briefly. A single absorption peak can be constructed taking the unrelaxed and relaxed moduli with respect to viscous shear relaxation and assuming a standard linear solid (i.e., using eq. 5). Compared to the absorption peaks obtained by the complete viscoelastic analysis (O'Connell and Budiansky, 1977, fig. 4) there exists no significant difference in the amplitude. However, the maxima of O'Connell and Budiansky's Q^{-1}-spectra are shifted slightly towards lower frequencies due to the SCS.

At crack densities corresponding to the case of complete wetting of grain faces O'Connell and Budiansky (1977) found Q^{-1} of viscous shear relaxation to range between 0.14 and 0.26. However, as was already pointed out by Nowick and Berry (1972), small irregularities of the grain faces could considerably inhibit a complete shear relaxation. Furthermore, if the corresponding relaxation times

are considered, viscous shear relaxation would account for measured Q^{-1} in the asthenosphere only if the melts have viscosities of 10^6–10^7 Pa s (Nur, 1971; Solomon, 1972). However, measured viscosities of silicate melts are between 1 and 1000 Pa s (Kushiro et al., 1976; Kushiro, 1977; and others). O'Connell and Budiansky (1977) therefore concluded that viscous shear relaxation was important for seismic frequencies only if the aspect ratios were smaller than 10^{-7}. This is demonstrated in Fig. 6 (top), where the characteristic frequencies are shown as a function of aspect ratio

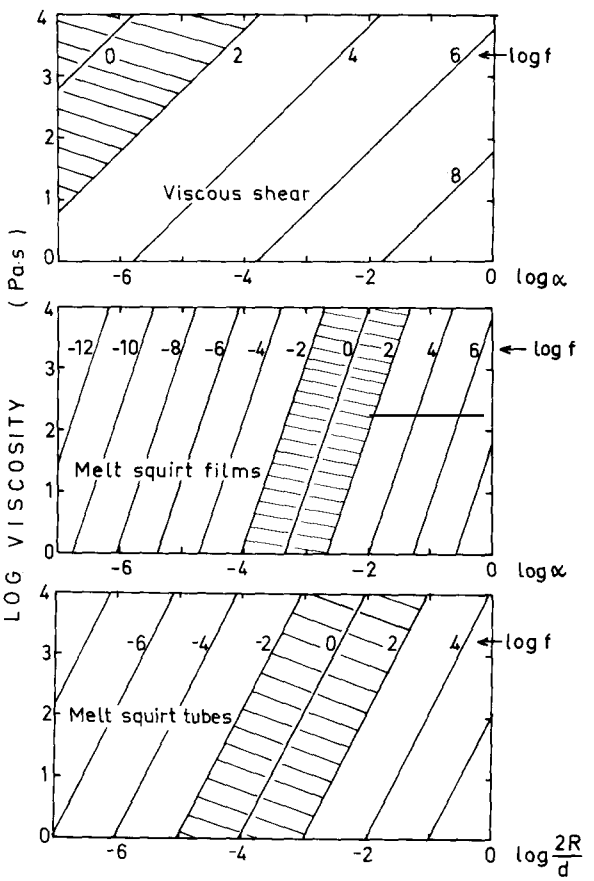

Fig. 6. Lines of constant relaxation frequencies as a function of log viscosity and log aspect ratio or $\log(2R/d)$, the equivalent aspect ratio for tubes. The numbers beside the curves refer to the log frequency f in Hz. Upper diagram: viscous shear relaxation. Central diagram: melt squirt in films. Lower diagram: melt squirt in tubes. Assumptions for the moduli: $K = 0.66$ Mbar, $\mu = 0.4$ Mbar, $K_f = 0.2$ Mbar.

and viscosity. The hatched area indicates the seismic band.

4.2.2. Melt squirt

Alternatively, pressure driven fluid flow is another potential mechanism of stress relaxation. Pressure variations may be produced within single inclusions if they deform non uniformly under an externally applied uniform stress. Such deformations of non-ellipsoidal dry cracks have been considered by Mavko and Nur (1978). Somewhat longer relaxation times are involved if the fluid flow takes place between neighbouring but interconnected inclusions. If the inclusions have a different geometry, say, a crack is connected with a spherical inclusion, an externally applied hydrostatic pressure will produce different fluid pressures in the two inclusions which, in turn, can equalize by flow. The corresponding relaxation frequency was estimated by Johnston et al. (1979). For typical bulk moduli and viscosities (see e.g., Kushiro et al., 1976; Stolper et al., 1981) the frequency ranges in the seismic band if the crack aspect ratio is smaller than 10^{-3}–10^{-2}.

Relaxation due to flow between interconnected inclusions of similar shape is possible if the externally applied stress is pure shear. Mavko and Nur (1975) introduced the term "melt squirt" for this mechanism. The fluid is squirted from inclusions oriented essentially perpendicular to the principle axis of compression to those essentially perpendicular to the principle axis of tension. O'Connell and Budiansky (1977) carried out a viscoelastic analysis of this mechanism for fluid filled cracks and estimated the characteristic frequency which is shown in Fig. 6 (centre). Melt squirt may be important in the seismic frequency range at aspect ratios $< 10^{-2}$–10^{-3}. O'Connell and Budiansky (1977) also calculated Q-spectra for distributed aspect ratios. They found that melt squirt could be important if the crack densities are sufficiently high for complete grain boundary wetting.

Mavko (1980) determined the relaxation due to melt squirt for the case in which melt occurs within tubes (Fig. 2c). He estimated the relaxation frequency for the case of tapered off cross sections ($\kappa = 0$, see Fig. 4). If the ratio length to the diameter of the tubes is smaller then 10^{-2}–10^{-3}, it is

possible that the frequency ranges in the seismic band (Fig. 6, bottom).

Based on the characteristic relaxation frequencies summarized in Fig. 6 it is assumed here that melt squirt is the only important relaxation mechanism due to melt at seismic frequencies. Thus, the term "unrelaxed" will be used only with respect to the melt squirt mechanism, and it is assumed that viscous shear relaxation has already taken place.

5. The complete set of melt models

5.1. The general equations

In this section a set of very general self consistent equations for the relaxed and unrelaxed moduli for a material containing arbitrary inclusions will be given. By utilizing published solutions for particular inclusion geometries a comprehensive set of equations is established with additional allowance for a varying degree of interconnection as well as superposition of melt geometries.

Since only melt squirt is considered here (see end of section 4.2.2) the unrelaxed modulus will be defined by the condition of no fluid exchange between inclusions. It is assumed that the pressure within each inclusion is uniform and no viscous shear stresses exist in the fluid. Different fluid pressures in different inclusions can then equalize by fluid flow if the inclusions are interconnected. The resulting isobaric state will be taken to define the relaxed moduli.

After Mavko (1980) the effective elastic moduli of a material containing arbitrary inclusions can be obtained by using the Betti–Rayleigh-reciprocity theorem (see e.g., Love, 1907, p. 205). It connects two arbitrary elastic states of equilibrium of a linear elastic body. If these two states 1 and 2 are represented by the surface displacements $\vec{\mathbf{u}}_1$, $\vec{\mathbf{u}}_2$ and the surface stress vectors or tractions $\vec{\mathbf{T}}_1$, $\vec{\mathbf{T}}_2$ acting on the body the theorem can be written

$$\int_F \vec{\mathbf{T}}_1 \vec{\mathbf{u}}_2 \mathrm{d}F = \int_F \vec{\mathbf{T}}_2 \vec{\mathbf{u}}_1 \mathrm{d}F \tag{18}$$

where the integration has to be carried out over the total outer and inner surfaces F.

The formulae of the different moduli for arbitrarily shaped, fluid filled inclusions being partly interconnected and partly isolated can be obtained by the following approach. The two states of stresses and displacements shown in Fig. 7 can be connected by the reciprocity theorem assuming linear elasticity. Figure 7a shows the body containing inclusions loaded by an external traction $\vec{\mathbf{T}}_e$. The inclusions "con" are regarded to be connected and thus allow for an equilibration of fluid pressures in the relaxed state. The inclusions "iso" are regarded to be isolated. $\vec{\mathbf{u}}$ and $\vec{\mathbf{v}}$ are the pore wall and body surface displacements. The individual pore pressures are indicated by p_{p1}, p_{p2},.... In Fig. 7b the pore walls are loaded with the tractions $\vec{\mathbf{T}}_i$, the same as the external $\vec{\mathbf{T}}_e$-tractions. Thus the resulting displacements $\vec{\mathbf{u}}_0$ and $\vec{\mathbf{v}}_0$ are the same as if the pores would contain solid matrix material. The two states of stress in Fig. 7 can be combined by the reciprocity theorem giving

$$\int_{F_e} \vec{\mathbf{T}}_e \vec{\mathbf{v}}_0 \mathrm{d}F + \sum_{i=1}^{N} \int_{f_i} p_{pi} \hat{\mathbf{n}} \vec{\mathbf{u}}_0 \mathrm{d}F = \int_{F_e} \vec{\mathbf{T}}_e \vec{\mathbf{v}} \mathrm{d}F + \sum_{i=1}^{N} \int_{f_i} \vec{\mathbf{T}}_i \vec{\mathbf{u}} \mathrm{d}F \tag{19}$$

where N is the total number of inclusions, F_e and f_i are the external and inclusion surfaces, and $\hat{\mathbf{n}}$ is the surface normal vector. As external tractions, either pure shear stress $\vec{\mathbf{S}}$ or hydrostatic pressure $P\hat{\mathbf{n}}$ are taken. The shear tractions are given by

$$\vec{\mathbf{S}} = \begin{pmatrix} S & 0 & 0 \\ 0 & -S & 0 \\ 0 & 0 & 0 \end{pmatrix} \hat{\mathbf{n}}$$

The specific strain energy represented by the first integrals on either side of (19) can be taken to define the undisturbed (matrix) and effective shear and bulk moduli, respectively

$$\frac{1}{\mu_0} = \frac{1}{VS^2} \int_{F_e} \vec{\mathbf{S}} \vec{\mathbf{v}}_0 \mathrm{d}F \quad \frac{1}{\mu_{\mathrm{eff}}} = \frac{1}{VS^2} \int_{F_e} \vec{\mathbf{S}} \vec{\mathbf{v}} \mathrm{d}F \tag{20a}$$

$$\frac{1}{K_0} = \frac{1}{VP^2} \int_{F_e} P \hat{\mathbf{n}} \vec{\mathbf{v}}_0 \mathrm{d}F \quad \frac{1}{K_{\mathrm{eff}}} = \frac{1}{VP^2} \int_{F_e} P \hat{\mathbf{n}} \vec{\mathbf{v}} \mathrm{d}F \tag{20b}$$

where V is the total volume.

To determine the unrelaxed moduli eq. 19 together with eq. 20 can be evaluated assuming that

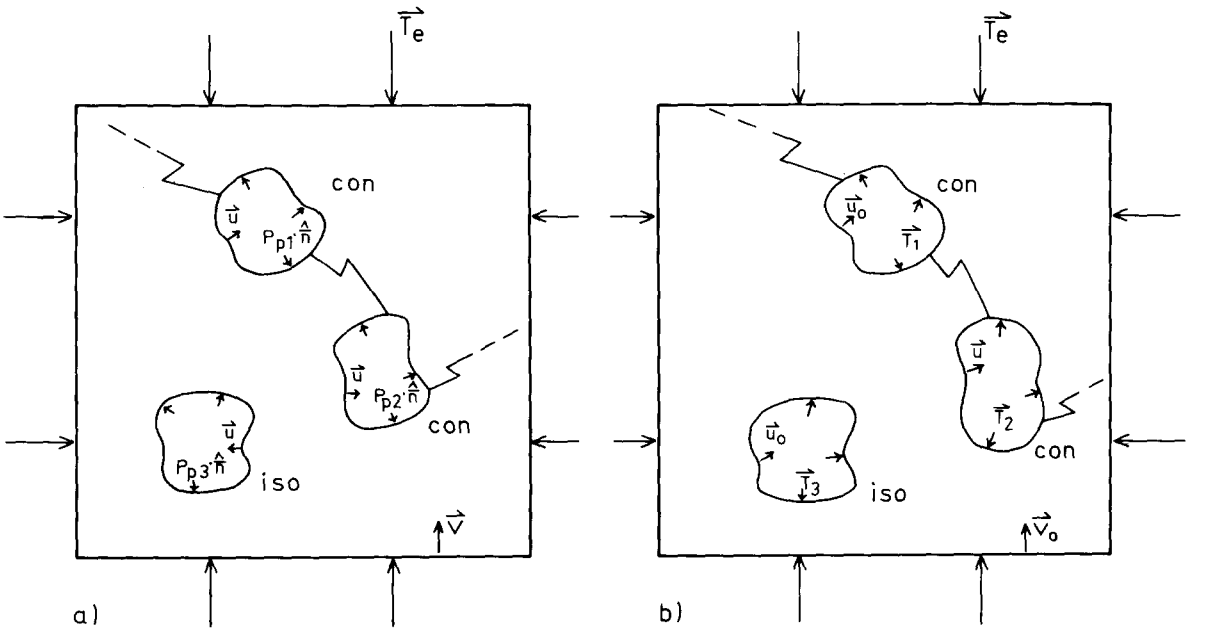

Fig. 7. Illustration for the reciprocity theorem. The inclusions "con." are assumed to be interconnected, those indicated by "iso." are isolated. For details, see text.

at the first instant of loading all inclusions are isolated. To take into account the SCS the resulting moduli are given together with the unrelaxed Poisson-constant ν in a set of coupled equations which have to be solved simultaneously

$$\frac{1}{K_u} = \frac{1}{K_0} + \frac{1}{V}\left(\frac{1}{K_f} - \frac{1}{K_0}\right) \sum_{i=1}^{N} \frac{V_i}{1 + \theta_i^{-1}\left(\frac{1}{K_f} - \frac{1}{K_u}\right)} \tag{21}$$

$$\frac{1}{\mu_u} = \frac{1}{\mu_0} - \frac{1}{S^2 V} \sum_{i=1}^{N} \int_{f_i} \bar{\mathbf{T}}_i \bar{\mathbf{u}} \, \mathrm{d}F \tag{22}$$

$$\nu_u = \frac{3K_u - 2\mu_u}{6K_u + 2\mu_u} \tag{23}$$

Here $\theta_i (= \int_{f_i} \bar{\mathbf{u}}\, \bar{\mathbf{n}} \, \mathrm{d}F / V_i P)$ represents the apparent compressibility of the i-th inclusion if it were dry and has to be determined for the particular inclusion geometries. $\theta_i = \theta_i(K_u, \mu_u)$ has to be determined for an inclusion embedded in a K_u-,μ_u-material. V_i is the volume of the i-th inclusion. For inclusions of similar shape (which then have the same pore pressure) (21) represents a self-consistent version of the Gassmann relation (Gassmann, 1951) (eq. A1, Appendix A). This relation gives the effective bulk modulus of a fluid-saturated body if the porosity and the bulk modulus of the fluid, the solid matrix, and the dry porous body are known. Note that (21) reduces to the original Gassmann-relation if the SCS is dropped, i.e., if K_u on the right-hand side is replaced by K_0 and $\theta_i = \theta_i(K_0, \mu_0)$. The derivation of (21) is given in Appendix A. In deriving (22) it has been taken into account that the second term in (19) vanishes if pure shear is assumed as the external traction.

To obtain the general equations for the relaxed moduli one has to distinguish between isolated and connected inclusions. It is assumed that in the second category the fluid pressure has equalized due to flow between pores (and is actually 0 for external pure shear) while the isolated pores retain the fluid with different individual pore pressures. Applying the reciprocity theorem gives the relaxed shear modulus as the solution of the coupled equa-

tions (where K' and ν' are auxiliary quantities)

$$\frac{1}{K'} = \frac{1}{K_0} + \frac{1}{V}\left(\frac{1}{K_f} - \frac{1}{K_0}\right) \sum_{i=1}^{N_{iso}} \frac{V_i}{1 + \theta_i^{-1}\left(\frac{1}{K_f} - \frac{1}{K'}\right)} + \frac{1}{V} \sum_{i=1}^{N_{con}} \theta_i V_i \tag{24}$$

$$\frac{1}{\mu_r} = \frac{1}{\mu_0} - \frac{1}{S^2 V}\left(\sum_{i=1}^{N_{iso}} \int_{f_i} \vec{T}_i \vec{u} \, dF \Big|_{K_f} + \sum_{i=1}^{N_{con}} \int_{f_i} \vec{T}_i \vec{u} \, dF \Big|_{K_f = 0} \right) \tag{25}$$

$$\nu' = \frac{3K' - 2\mu_r}{6K' + 2\mu_r} \tag{26}$$

The sums in (24) and (25) have to be extended over the isolated (N_{iso}) and the interconnected (N_{con}) inclusions, respectively. Here θ_i has to be taken as a function of K' and μ_r. In the first integral of (25) fluid filled inclusions are assumed while dry pores have to be considered in the second integral. To determine the relaxed bulk modulus Gassmann's (1951) relation can be used in the form

$$K_r = K_{iso} \frac{K' + F}{K_{iso} + F} \quad \text{with} \quad F = \frac{K_f (K_{iso} - K')}{\beta_c (K_{iso} - K_f)} \tag{27}$$

Here K_{iso} has to be determined simultaneously with a quantity μ_{iso} using eqs. 21–23 by summing only over the isolated inclusions and reducing V by the total volume of the interconnected pores. β_c represents the volume concentration of the interconnected pores.

The sums occurring in the set of eqs. 21–25 can be evaluated for particular inclusion geometries. It seems reasonable to model a range of geometries as broad as possible for a partially molten rock by allowing for film, tubular, and spheroidal shaped inclusions. If these geometries are denoted by the subscripts $m = 1, 2, 3$, respectively, and the corresponding melt fractions of the isolated and connected inclusions by β_i and β_c, respectively, the equations can be written as

$$\frac{1}{K_u} = \frac{1}{K_0} + \sum_{m=1}^{3} \frac{\left(\frac{1}{K_f} - \frac{1}{K_0}\right)(\beta_{mi} + \beta_{mc})}{1 + \theta_m^{-1}(K_u, \mu_u, \nu_u)\left(\frac{1}{K_f} - \frac{1}{K_u}\right)} \tag{28}$$

$$\frac{1}{\mu_u} = \frac{1}{\mu_0} + \sum_{m=1}^{3} A_m(K_u, \mu_u, \nu_u, K_f).(\beta_{mi} + \beta_{mc}) \tag{29}$$

$$\nu_u = \frac{3K_u - 2\mu_u}{6K_u + 2\mu_u} \tag{30}$$

2 my_u

$$\frac{1}{K'} = \frac{1}{K_0} + \sum_{m=1}^{3} \left(\frac{\left(\frac{1}{K_f} - \frac{1}{K_0}\right)\beta_{mi}}{1 + \theta_m^{-1}(K', \mu_r, \nu') \cdot \left(\frac{1}{K_f} - \frac{1}{K'}\right)} + \theta_m(K', \mu_r, \nu') \cdot \beta_{mc} \right) \tag{31}$$

$$\frac{1}{\mu_r} = \frac{1}{\mu_0} + \sum_{m=1}^{3} \left(A_m(K', \mu_r, \nu', K_f) \cdot \beta_{mi} + A_m(K', \mu_r, \nu', K_f = 0) \cdot \beta_{mc} \right) \tag{32}$$

$$\nu' = \frac{3K' - 2\mu_r}{6K' + 2\mu_r} \tag{33}$$

K_r is obtained by using (27) where K_{iso} has to be determined with μ_{iso} from (28) to (30) assuming a modified total melt fraction $\beta'_m = \beta_{mi}/(1 - \beta_{mc})$. The quantities θ_m and A_m ($m = 1, 2, 3$) for the particular geometries can be taken from O'Connell and Budiansky (1977), Mavko (1980) and Wu (1966). They are listed in Appendix B.

The above set of equations gives the moduli necessary to determine the relaxation strength for shear, Δ_μ, and for compression Δ_K, according to eq. 4 or the maximum Q^{-1} denoted by $\Delta'_\mu/2$ and $\Delta'_K/2$ according to (5). However, since the derivations of the relaxed and unrelaxed bulk modulus are based on different approaches care has to be taken when their difference is small, i.e., when Δ_K

is small. It should be mentioned that for melt films also distributed aspect ratios can be considered using the representative aspect ratio α' as given in eq. 17. In the following three sections the theory for melt inclusion models is extended with regard to general ellipsoidal inclusions, variable degree of interconnection between inclusions, and combination of inclusions of different geometry.

5.2. *Moduli and relaxation strength for ellipsoidal inclusions*

5.2.1. *Triaxial inclusions*

In the viscoelastic models by O'Connell and Budiansky (1977) and Walsh (1969) the melt films were approximated by ellipsoidal inclusions having a small aspect ratio $\alpha(\ll 1)$. However, as has been pointed out in section 4.1., it is questionable whether such small values of α are reasonable. The elastic solutions for ellipsoidal inclusions given by Wu (1966), Kuster and Toksöz (1974) and Korringa et al. (1979) allow for arbitrary aspect ratios. However, these solutions do not consider triaxial ellipsoids ($a \neq b \neq c$); furthermore, they do not consider relaxation. To account for these extra factors the model presented here gives the relaxed and unrelaxed moduli and the relaxation strength for ellipsoidal inclusions with the half axes $a \geq b \geq c$. Whether the case $a \neq b \neq c$, as was shown for films by O'Connell and Budiansky (1974), can be reduced to the case $a' = b' \neq c$ by using relation (16) will be tested numerically.

The set of eqs. 21–27 has been taken to determine the effective moduli for ellipsoidal inclusions of the same shape assuming complete interconnection. For this case the pore wall displacements can be determined by using the results of Eshelby (1957). Eshelby gave the solutions for the strain of an inclusion if a uniform arbitrary stress is applied at infinity. Assuming either pure shear or uniform compression at infinity, Eshelby's expressions were solved numerically to give the integrals over the pore wall displacements. These were integrated numerically over all possible orientations of the inclusions to give the effective moduli. The numerical accuracy of the multiple integrations was tested by known analytical solutions for disc-, needle-, and spherical shaped inclusions and turned out to be better than 0.5%.

The numerical solutions have been used to test the conditions in which triaxial ellipsoids with the axes a, b, c can be reduced to the case $a' = b' \neq c$. For different b/a-ratios a' was determined according to (16). With this a' an α' was defined as $\alpha' = c/a'$. Numerical determinations of effective moduli and relaxation strengths have been carried out by varying b/a for different α' and melt concentrations. Figure 8 shows some results for the unrelaxed shear modulus (where the undisturbed modulus was 0.4 Mbar). Since the abscissa gives b/a, the curves for the moduli and relaxation strengths should be horizontal if (16) is applicable to ellipsoidal inclusions with finite thickness. The deviation from horizontal increases with α' and with melt concentration. From Fig. 8 it can be

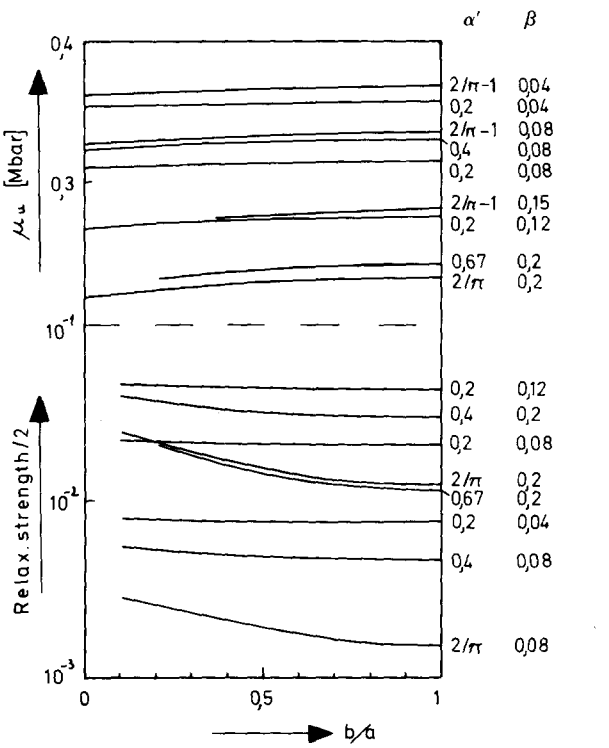

Fig. 8. Unrelaxed shear modulus (upper part) and half relaxation strength $\Delta'/2$ (lower part) for ellipsoidal inclusions with three different axes $a \geq b \geq c$ as a function of b/a. $\alpha' = c/a'$ and β give the particular aspect ratios and melt fractions. Assumptions for the moduli: $K_0 = 0.66$ Mbar, $\mu_0 = 0.4$ Mbar, $K_f = 0.2$ Mbar, $\mu_f = 0$. The SCS was applied.

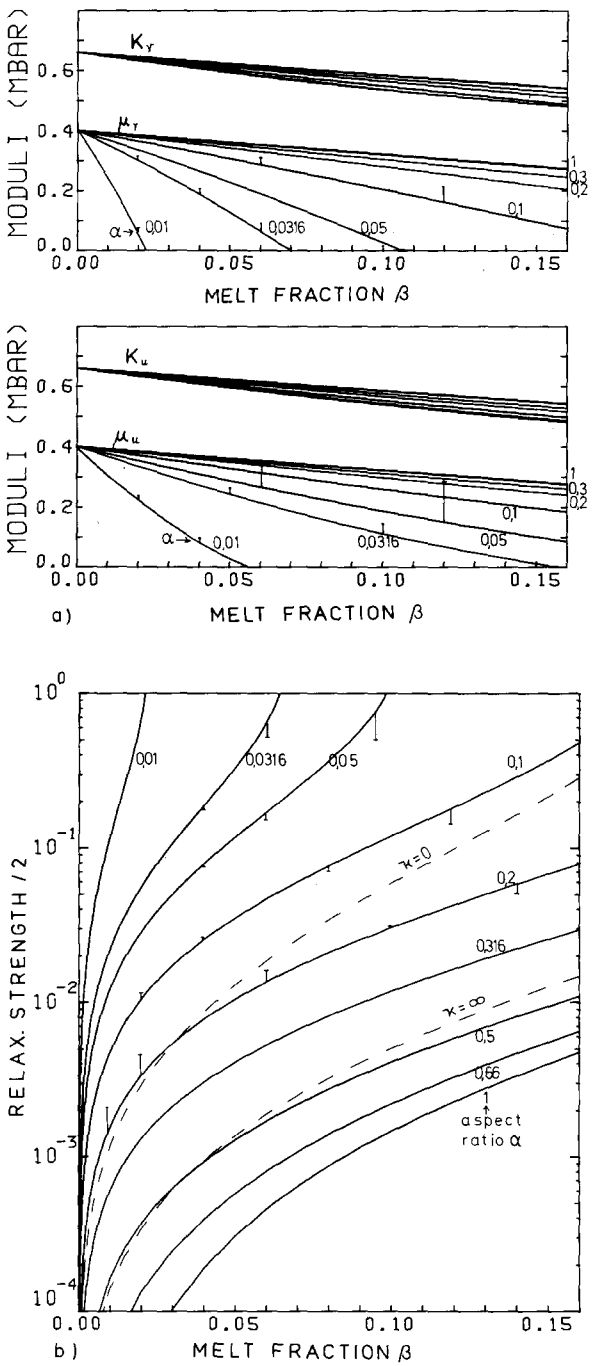

Fig. 9. (a) Relaxed (top) and unrelaxed (bottom) moduli for ellipsoidal inclusions. The numbers beside the curves give the aspect ratios. The bars indicate the deviation from O'Connell and Budiansky's (1977) film model (and are omitted for $\alpha \geq 0.2$). (b) Half shear relaxation strength $\Delta'/2$ for ellipsoidal (spheroidal) inclusions (solid curves) and melt tubes (dashed curves). The numbers give the aspect ratio, κ gives the shape of the tubular cross section. The bars give the deviation from the film model. The undisturbed moduli are the same as in Fig. 8.

inferred that (16) appears to be applicable for $\alpha' < 0.2$. For $\alpha' > 0.2$ the condition (16) is only applicable if, with decreasing α', a decrease of the moduli of a few percent and an increase of the relaxation strength up to a factor of two is taken into account.

5.2.2. *Spheroidal inclusions*

The extension of (16) towards finite aspect ratios is regarded to be sufficiently accurate to drop the complicating assumption of three different axes and, instead, to consider ellipsoids with two equal axes $a = b \neq c$ (i.e., spheroids). The analytical eqs. 28–33 (plus 27) are applied for the particular case of completely interconnected spheroidal inclusions. (5) was used to determine $\Delta'/2$ for shear which gives approximately the half shear relaxation strength.

Figure 9 shows the decrease of the unrelaxed and relaxed shear and bulk modulus and $\Delta'/2$ with increasing melt fraction for different aspect ratios. After Berckhemer et al. (1982a) and Stolper et al. (1981) the following values have been chosen to represent partially molten ultrabasic rocks under room pressure: $K_0 = 0.66$ Mbar, $\mu_0 = 0.4$ Mbar, $K_f = 0.2$ Mbar, $\mu_f = 0$. The self-consistent scheme was applied. The vertical bars indicate the deviation from the film model of O'Connell and Budiansky (1977) who considered infinitely thin cracks when determining the reduction of strain energy due to the cracks. For $\alpha \leq 0.01$ the present models agree well with the film model, however, above $\alpha = 0.03$ finite inclusion thickness influences the elasticity significantly. It is noteworthy that for aspect ratios between 0.2 and 1 the moduli do not differ very much. This suggests that, so long as the melt pockets have a convex shape, the elastic behaviour of a material containing melt pockets of different shape does not differ significantly from a material having completely spherical inclusions. The vertical bars in Fig. 9b indicate that the relaxation strength (actually $\Delta'/2$) does not show a pronounced departure from the film model. The

deviations in moduli partially cancel out when taking the difference between μ_u and μ_r as required by (5). Figure 9b shows that high relaxation strengths are obtained for arbitrarily small melt fractions as long as the aspect ratio is sufficiently small. However, for $\alpha > 0.1$, significant melt fractions are required for high values of relaxation strength. In contrast to the moduli themselves, $\Delta'/2$ depends significantly on the aspect ratio between α-values of 0.2 and 1.

An interesting result is the finite relaxation strength for spherical inclusions ($\alpha = 1$). Under an external load one would expect the fluid pressure in all spheres to be equal (or zero in the case of pure shear) because no relaxation due to pressure induced flow should be possible. In fact the finite $\Delta'/2$ is a consequence of the SCS which is used to approximate the interactions between inclusions. This can be illustrated by considering a spherical inclusion being influenced by an external pure shear of magnitude p (Fig. 10). According to Eshelby's (1957) solutions the pressure in the surrounding material at a (b) can be determined to be $+(-)\ 5\ p(1+\nu)/(7-5\nu)$ where ν is the Poisson-ratio. Thus, an imaginary neighbouring inclusion near point a will show a lower fluid pressure than one near b; such differences would be equalized by fluid flow if they were interconnected.

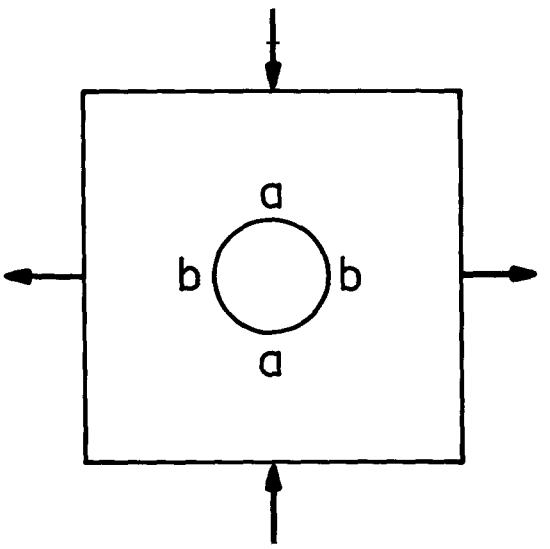

Fig. 10. See text.

Figure 11 shows a possible combination of the results shown in Fig. 9. Such a diagram could be used to interpret in situ data of particular regions of the asthenosphere in terms of melt fraction and geometry if estimates of the relaxation strength and the reduction of the shear modulus due to melt are given from seismic data. The shear relaxation strength (actually $\Delta'/2$) is plotted versus the unrelaxed shear modulus which in turn decreases below the undisturbed value of 0.4 Mbar as the melt fraction increases. The uppermost curve represents extremely thin films. Finite aspect ratios result in lower curves. For thin melt films a particular data pair of Δ', μ_u on the upper curve may result from different melt fractions β and aspect ratios α as long as their *ratio* α/β (i.e., "crack density") is equal. However, for finite aspect ratios there exists an unequivocal relationship between the four quantities Δ', μ_u, α, β. Hence, if both the

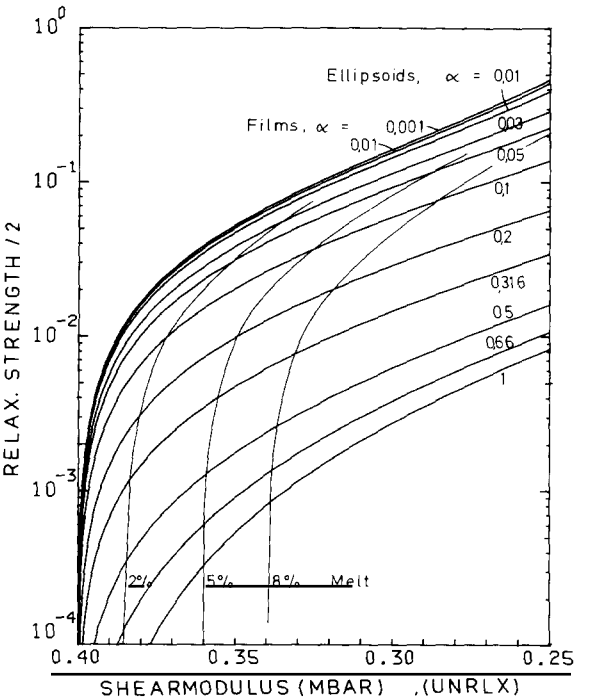

Fig. 11. Half shear relaxation strength $\Delta'/2$ as a function of the decreasing unrelaxed shear modulus for ellipsoidal (spheroidal) inclusions and films. The curves 2%, 5% and 8% give the melt fractions leading to the modulus decreases and relaxation strengths shown. The undisturbed moduli are the same as in Fig. 8.

relaxation strength and the shear modulus are given, it is possible to determine both the aspect ratio and the melt fraction assuming ellipsoidal inclusions. Three lines of corresponding melt fractions are shown.

An interesting feature arises from the diagram: if the modulus decrease is fixed, high relaxation strength (absorption) results from low melt fractions and vice versa.

For comparison Fig. 12 shows the melt model for tubes from Mavko (1980) in a representation corresponding to Fig. 11. The curves for the different cross-sections are similar to those for ellipsoidal inclusions with aspect ratios between 0.2 and 0.5, however, the melt fractions are higher.

If the spheroidal inclusions are chosen to be prolate ($a \geq b = c$), the shear relaxation strength does not change more than by a factor of three and there is only a narrow range of effective moduli between the spherical and the tubular case. The range is approximately the same as that

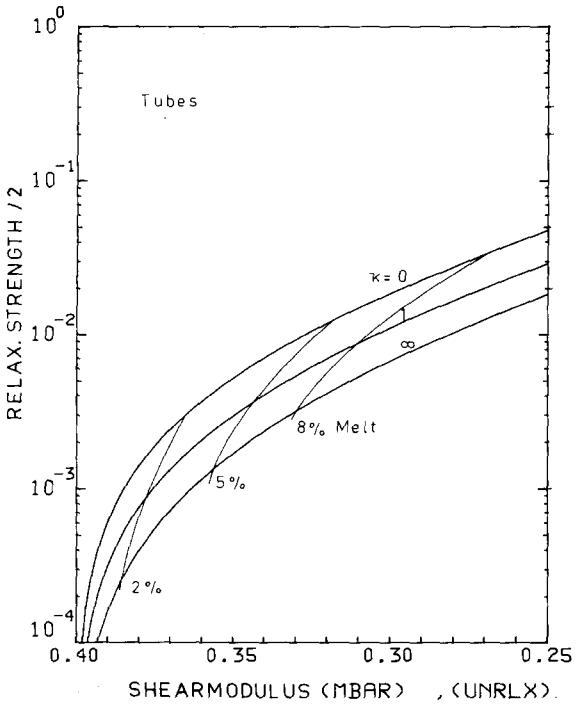

Fig. 12. The same as Fig. 11, but for melt tubes with the shape parameter $\kappa = 0, 1, \infty$.

covered by oblate spheroids with α between 0.3 and 1 (Fig. 9).

For the above models certain typical elastic moduli M_0 and K_f have been chosen. It should be mentioned that these undisturbed moduli can be regarded as normalizing quantities as long as the undisturbed Poisson-ratio ν_0 does not deviate too much from 0.25. Thus, the results can be transferred to other materials and pressure conditions. However, varying K_f with respect to K_0 significantly influences the effective bulk modulus, while the shear modulus and the corresponding relaxation strength are affected only slightly so long as $K_f/K_0 \geq 0.15$.

5.2.3. The influence of a reduced degree of interconnection

Assuming that the melt does not fracture its surroundings when a seismic wave is passing through, seismic absorption (or relaxation) by melt flow can only occur through interconnected pores; isolated melt inclusions are not involved in melt squirt. The unrelaxed moduli are completely independent of the connectiveness. By contrast, the relaxed moduli, and especially the shear relaxation strength, depend strongly on the degree of interconnection of melt inclusions. Schmeling (1983, and in prep.(b)) developed a statistical model to describe the connectiveness of a system of randomly oriented and distributed ellipsoidal inclusions or films (with the axes $a = b \neq c$). The degree of interconnection, ζ, is defined as the fraction of inclusions which overlap at least with one of the neighbouring inclusions. The statistical model determines ζ as a function of β and α. As a result, lines of constant ζ are shown in Fig. 13b. Figure 13a illustrates the basic idea of this model. The degree of interconnection $\zeta(\alpha, \beta)$ can be used to define the portions of melt fractions in eqs. 28–33 representing isolated and interconnected pores, β_i and β_c. The total melt fraction, β, can be written

$$\beta = (1 - \zeta)\beta_i + \zeta\beta_c$$

Effective moduli and shear relaxation strength have been determined by taking ζ from the diagram of Fig. 13. Figure 14 shows the departure of the relaxation strength from the case of complete in-

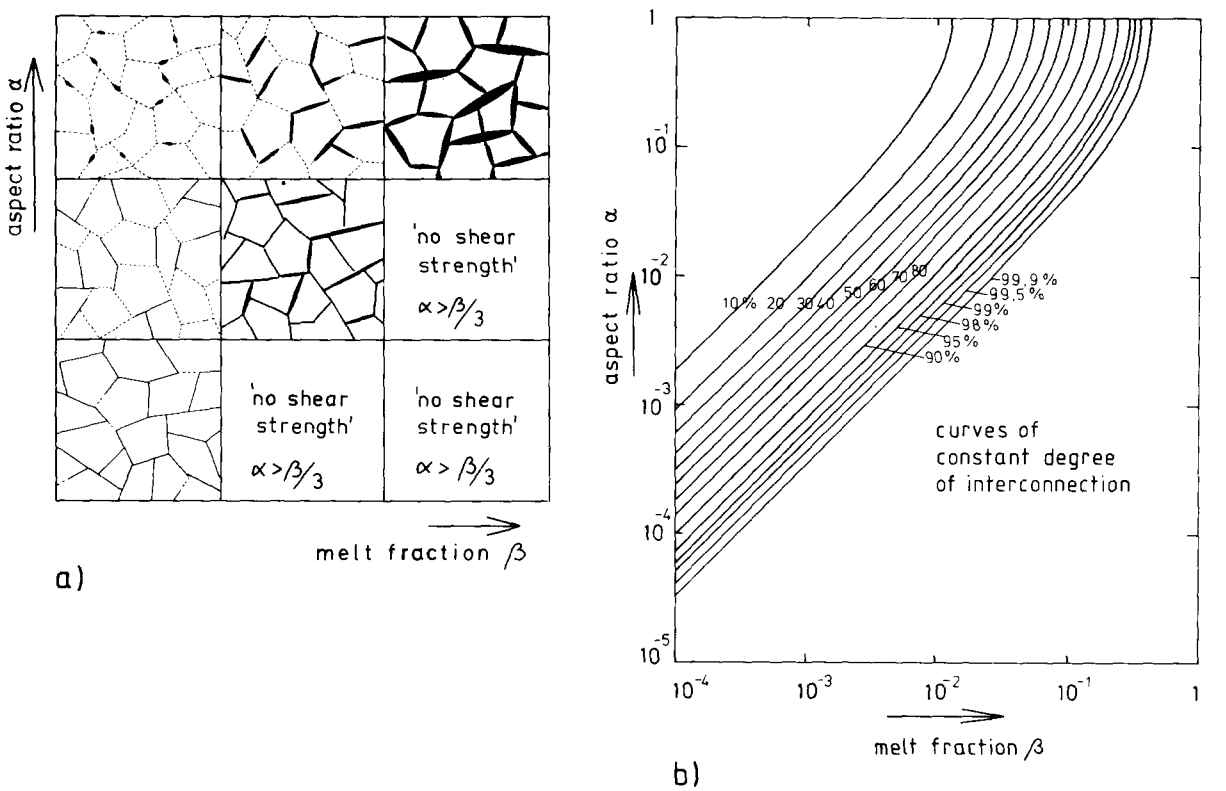

Fig. 13. (a) Illustration of the variable degree of interconnection for ellipsoidal (spheroidal) inclusions as a function of melt fraction β and aspect ratio α. The quotes indicate the idealistic nature of this model, since in nature irregularities at the film faces could prevent a complete loss of shear strength at small melt fractions. (b) Curves of constant degree of interconnection as resulting from the statistical model of overlapping of penny shaped or ellipsoidal (spheroidal) inclusions. The numbers at the curves give the total probability of overlapping with neighbouring inclusions.

terconnection (dashed curves) for melt films and spheroidal inclusions. For strong modulus decrease (right part of curves) the melt fraction is high and, thus, ζ is high. The relaxation strength approaches the dashed curves. However, at low melt fractions, i.e., for only slightly decreased moduli, ζ is low and the relaxation strengths differ significantly from those of the interconnected case. It should be emphasized that in situ determinations of the decrease of the shear modulus in the oceanic asthenosphere appear to lie well around 10% (Schmeling, 1984; and in prep.(a)). Thus, the possibility of a reduced degree of interconnection and a corresponding decrease of the relaxation strength due to melt should therefore be kept in mind.

5.3. Superposition of different melt geometries

The set of eqs. 28–33 allows the superposition of different inclusion geometries. A number of possible combinations of superpositions have been discussed by Schmeling (1983). Here only the most interesting one, i.e., that of melt films plus spherical inclusions, is considered. For simplicity a complete degree of interconnection has been assumed. The aspect ratio for the films was chosen to be 0.01. Figure 15a shows the effective unrelaxed moduli, μ, K, and $K + 4/3\,\mu$ (= modulus for P-waves) as a function of melt fraction for different volumetric fractions of melt in films and in spheres (given in percent of the total melt fraction). As expected a gradual transition in the moduli occurs from the

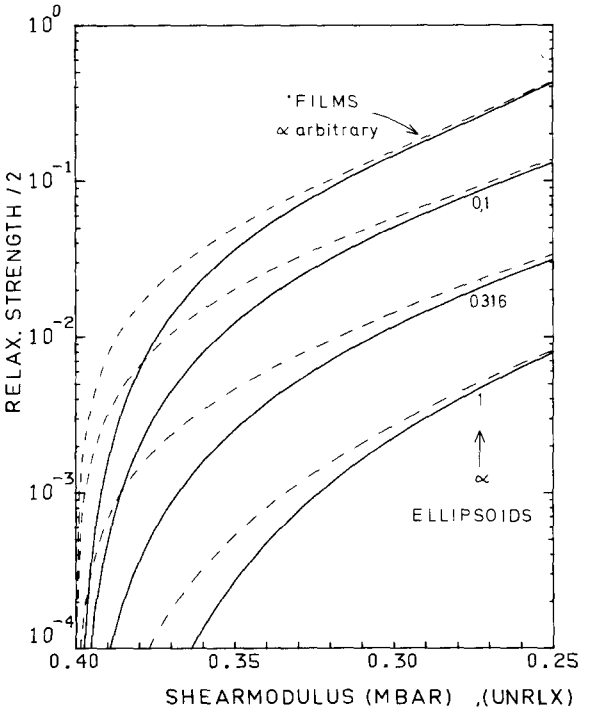

Fig. 14. Half shear relaxation strength $\Delta'/2$ as a function of the decreasing unrelaxed shear modulus for films and spheroids. The solid curves take into account a reduced degree of interconnection according to Fig. 13, while the dashed curves assume complete interconnection.

curves for spheres to those for films. Figure 15b shows the shear relaxation strength ($\Delta'/2$) as a function of the decreasing unrelaxed shear modulus. Starting with the case of spheres, there is a drastic increase of the relaxation strength if a small amount of melt occurs in films. 5% of the melt in films leads to an increase in Δ' of one order of magnitude. However, this is quite natural since the relaxation for the case of spheres is based only on the elastic interaction of the spheres and would not occur without the application of the SCS. On the other hand, it is clear from Fig. 15b that quite a lot of melt is needed in pockets to reduce the relaxation strength considerably below that for films. It should be noted that the curves for $5\%F$ and $1\%F$ are very sensitive to the aspect ratio of the films. The three curves 2%, 5% and 8% indicate the corresponding total melt fractions.

A very interesting aspect arises from the bulk relaxation strength shown in Fig. 15c. Almost no relaxation occurs if only one inclusion shape is present because the relaxation depends only on the coupling between K_u and μ_u (and K_r and μ_r) as a consequence of the SCS (see curve for 100% S). If melt occurs only in films the behaviour of the bulk relaxation strength is indicated by the curve 100% F. Δ increases generally with melt fraction. However, when the relaxed shear modulus reaches 0, the coupling between K and μ decreases until eventually μ_u also reaches 0. No further coupling occurs and so Δ also approaches 0. Such a material without shear strength ($\mu = 0$) represents a suspension with free fluid flow. Hence different fluid pressures do not occur which could equilibrate by relaxation.

If films and spheres are superimposed, the bulk relaxation strength increases significantly. Apparently there exists a certain ratio of films to spheres where the relaxation strength is maximum. The reason for this high relaxation strength lies in different fluid pressures due to different pore geometries. As a comparison the dashed curve in Fig. 15c gives the shear relaxation strength.

The mechanism of bulk relaxation was pointed out earlier by Johnston et al. (1979). Budiansky and O'Connell (1980) gave quantitative results, but only for 5% volumetric fraction of spheres, a crack density of 0.1, and a fluid bulk modulus of 0.5 K_0. They calculated the frequency dependent ratio Q_K^{-1}/Q_μ^{-1} ranging between 0.05 and 0.5. However, as has been pointed out by Schmeling (1983) the ratio of the relaxation strength Δ'_K/Δ'_μ, and hence also of Q_K^{-1}/Q_μ^{-1}, is sensitive to the total melt fraction, the ratio between β_f and β_s (the melt fractions of the films and of the spheres), and K_f. The dependence of Δ'_K/Δ'_μ on β and on β_f/β_s can be seen by relating the dashed curve for shear relaxation to those for bulk relaxation in Fig. 15c. The dependence on K_f may be described briefly by noting that the bulk relaxation strength for $\beta_f/\beta_s = 10/90$ increases roughly by one order of magnitude if K_f decreases from 0.5 K_0 to 0.15 K_0. If the above parameters are chosen properly (e.g., $K_f \cong 0.15\ K_0$, $\beta_f/\beta_s \cong 10\alpha$, and $\beta < 15\%$) it is even possible to obtain shear and bulk relaxation strengths of the same order of magnitude.

6. General discussion and conclusions

This paper has tried to establish a comprehensive set of elastic and anelastic models with melt inclusions covering a considerably broad range of melt geometries. In particular melt is assumed to occur in ellipsoidal inclusions with arbitrary combinations of half axes, in thin films, and in tubes of different cross-sections. Furthermore superpositions of these geometries are possible and the degree of interconnection can be varied. However, it is clear that the above inclusion geometries represent only idealized cases. In particular, the ellipsoidal melt pockets have a convex shape while in nature concave tetrahedrons are possible as well (see Fig. 2c or d). The effect of compact inclusions with concave curvature and sharp edges can be assessed roughly by comparing the different tube models with concave and convex cross-sections (Figs. 4 and 12).

It should be emphasized that melt squirt was regarded as the only important relaxation mechanism due to partial melt. Viscous shear relaxation was considered by O'Connell and Budiansky (1977). Relaxation due to phase changes and thermoelasticity can also lead to high relaxation strengths, particularly in compression (Vaisnys, 1968; Kjartansson, 1979; Mavko, 1980). However, although the characteristic frequencies of these effects are difficult to estimate, they appear to lie below the seismic frequency band. Absorption in the solid phase appears to be present almost independently of melt at low melt fractions and is found to dominate over the above mechanisms (Berckhemer et al., 1982a; Kampfmann, 1984; see also Schmeling, 1983).

The melt was assumed to be distributed isotropically in this study. However, a preferred orientation of grains and of melt inclusions might have been established in partially molten regions which are subjected to regional stresses. Such anisotropy would result in an anisotropic decrease of the effective moduli (Anderson et al., 1974), while melt squirt relaxation would be less efficient.

The models considered here allow the following conclusions:

(1) triaxial ellipsoidal inclusions can be approximated by spheroidal inclusions ($a = b \neq c$) if relation (16) is used;

(2) O'Connell and Budiansky's (1977) film model is accurate up to aspect ratios of $\cong 0.03$;

(3) for aspect ratios between 0.2 and 1 melt squirt relaxation is small and the effective moduli do not vary significantly with aspect ratio;

(4) a reduced degree of interconnection would be of importance in reducing the relaxation strength, and thus Q^{-1}, especially at melt concentrations leading to a moderate modulus (or v_p) decrease;

(5) if different melt geometries are present in the same rock, the bulk relaxation strength increases significantly. Under certain conditions it may reach the order of the shear relaxation strength; and

(6) it has been found to be useful to represent the melt models by plotting the relaxation strength as a function of the modulus decrease (Figs. 11, 12 and 15b). This allows a clear distinction between the effects of different melt geometries. Furthermore, such diagrams can be used easily for the simultaneous interpretation of observed values of Q^{-1} and of seismic velocity decreases.

The basic idea of the present paper was to provide a comprehensive set of elasticity and relaxation melt models which could be combined with corresponding melt models for the electrical conductivity. Such a set of models was developed by Schmeling (1983) and will be presented in part II of this paper. By combining these sets of models it is possible to carry out a combined interpretation of seismic and electrical conductivity data from partially molten mantle regions (Schmeling, 1983, 1984, 1985). To apply the models to observational data the following conditions should be fulfilled: seismic velocities of the anomalous region under consideration should be available, together with estimates of the velocities of the unmolten material. If Q^{-1}-data are available, these can be used to limit an upper boundary for the relaxation strength due to partial melt. It should be noted that laboratory measurements indicate that seismic absorption seems to be dominant in the solid phase at high temperatures, while the modulus decrease appears to be controlled by the melt (Berckhemer et al., 1982a,b; Kampfmann, 1984). To estimate the in situ relaxation strength,

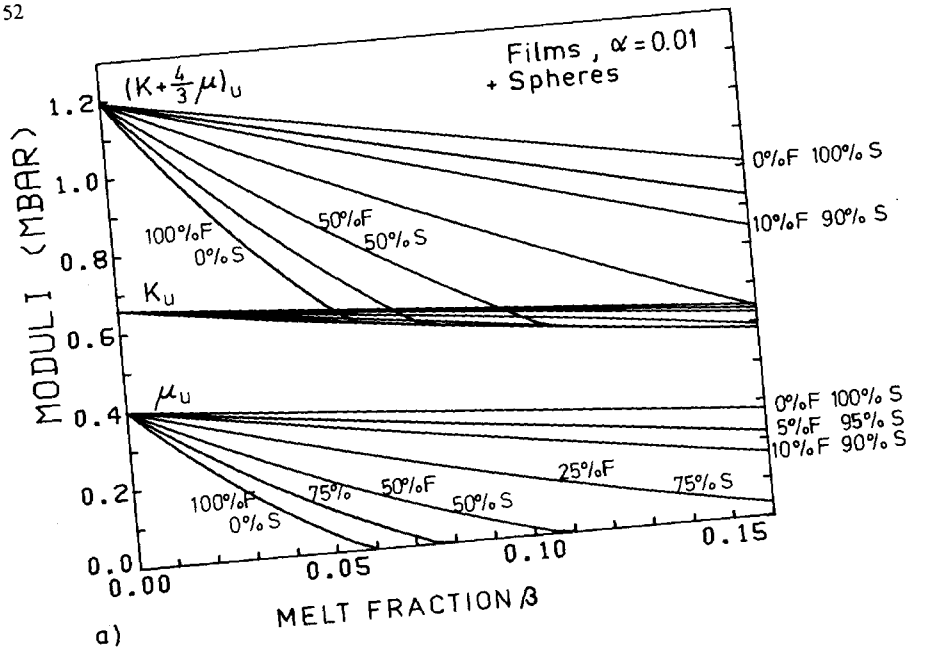
Films , α = 0.01
+ Spheres
$(K+\frac{4}{3}\mu)_U$
K_U
μ_U
MODULI (MBAR)
MELT FRACTION β
0%F 100% S
10%F 90% S
100%F 0%S
50%F 50% S
0%F 100% S
5%F 95% S
10%F 90% S
25%F 75% S
100%F 0%S
75% 50%F 50% S
75% S
1.2
1.0
0.8
0.6
0.4
0.2
0.0
0.00
0.05
0.10
0.15

a)

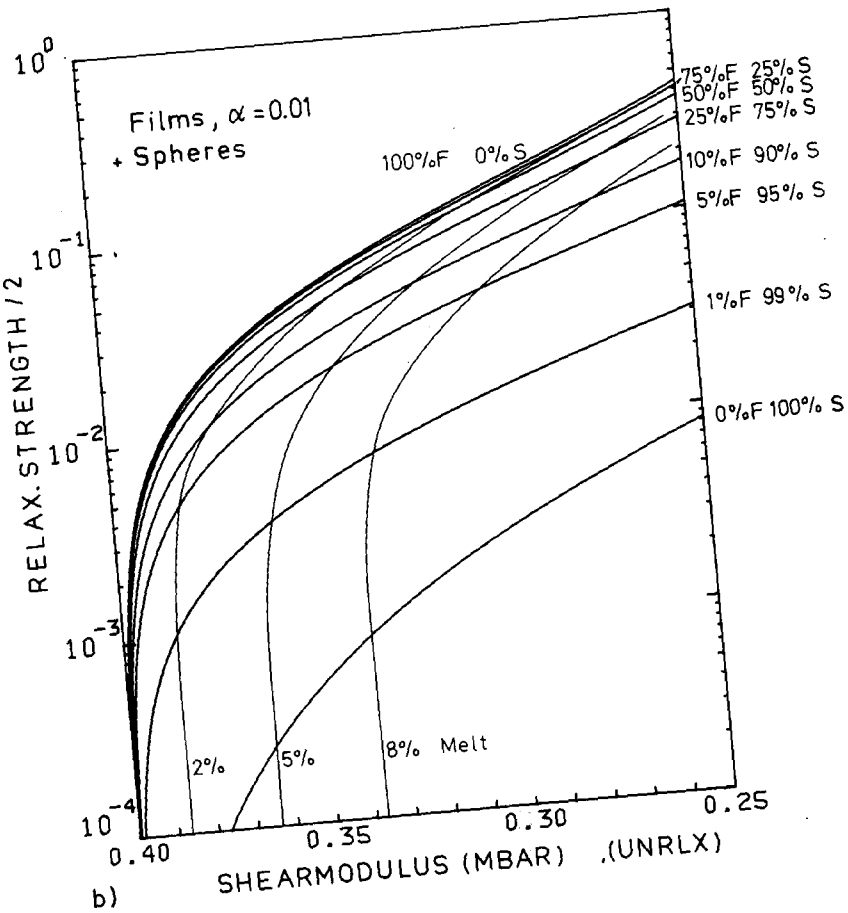
Films , α = 0.01
+ Spheres
100%F 0% S
75%F 25% S
50%F 50% S
25%F 75% S
10%F 90% S
5%F 95% S
1%F 99% S
0%F 100% S
RELAX. STRENGTH / 2
SHEARMODULUS (MBAR) (UNRLX)
2%
5%
8% Melt
10^{0}
10^{-1}
10^{-2}
10^{-3}
10^{-4}
0.40
0.35
0.30
0.25

b)

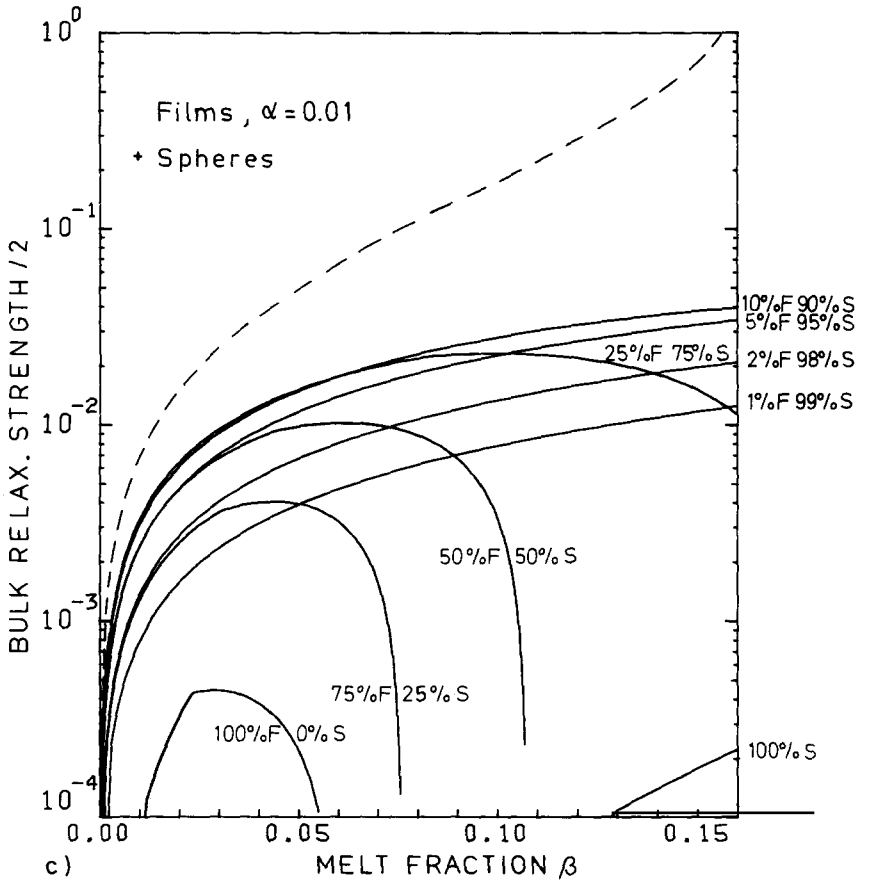

Fig. 15. Superposition of melt films ($\alpha = 0.01$) with spherical inclusions. The numbers in $\%F$ and $\%S$ give the volumetric fraction of the films and spheres with respect to the total melt fraction. The undisturbed moduli are the same as in Fig. 8. (a) Unrelaxed moduli. (b) Half shear relaxation strength $\Delta'/2$ as a function of the decreasing unrelaxed shear modulus. (c) Half bulk relaxation strength $\Delta'/2$ as a function of the total melt fraction. Dashed: $\Delta'/2$ (for shear) for the combination $10\%F$ and $90\%S$.

information about the absorption band is desirable. Furthermore the absorption band could be used to estimate the unrelaxed moduli, which in turn does not depend on frequency dependent relaxation. Finally, observations of the electrical conductivity have the potential of putting stronger constraints on the fractions and geometries of melt in anomalous mantle regions (Schmeling, 1985).

Acknowledgements

I am grateful to H. Berckhemer for his helpful and stimulating discussions and suggestions, and my wife, G. Marquart, for useful comments during the preparation of this work. C. Talbot read the manuscript and offered helpful comments. Financial support from the Deutsche Forschungsgemeinschaft under grant number Be 299/59 is gratefully acknowledged.

Appendix A

Self consistent bulk modulus and Gassmann's relation

To obtain the bulk modulus Mavko (1980) applied Gassmann's (1951) relation both for the re-

laxed and the unrelaxed moduli. This relation gives the effective bulk modulus of a saturated porous material, K_s, in which the fluid pressure is assumed to be constant throughout the pore-space

$$K_s = K_0 \frac{K_d + F}{K_0 + F} \quad F = \frac{K_f \cdot (K_0 - K_d)}{\beta \cdot (K_0 - K_f)} \tag{A1}$$

where K_f, K_0, and K_d are the bulk moduli of the fluid, of the solid matrix and of the dry porous body, respectively. Here a self-consistent derivation of K_s is presented which takes into account the possibility of different pore pressures. It is assumed that the apparent compressibility of a dry pore of volume V_i, $\theta_i = (V_i P)^{-1} \int_{f_i} \vec{u}\, \hat{\vec{n}} \mathrm{d}F$, under an external compression, P, is known if the inclusion were embedded in a medium with the moduli K and μ: $\theta_i(K,\mu)$. If a material containing N isolated inclusions filled with a fluid of bulk modulus K_f is loaded externally by hydrostatic compression, $\vec{T} = P\hat{\vec{n}}$, a pore pressure p_{pi} will develop in the i-th pore. Applying the reciprocity theorem (Fig. 7) and using (19) and (20b) one obtains for the effective saturated bulk modulus

$$\frac{1}{K_s} = \frac{1}{K_0} + \frac{1}{PV} \sum_{i=1}^{N} \frac{\delta V_i}{V_i} V_i + \frac{1}{P^2 V} \sum_{i=1}^{N} \int_{f_i} p_{pi} \hat{\vec{n}} \vec{u}_0 \mathrm{d}F \tag{A2}$$

Here $\delta V_i / V_i$ is the relative change in volume of the i-th saturated pore. The pore pressure in the last term in (A2) is constant and can be written in front of the integral. The remaining integral gives the volume change of the i-th pore as if it were filled with K_0-material. Thus we have $\int_{f_i} \hat{\vec{n}} \vec{u}_0 \mathrm{d}F = -V_i P / K_0$ and can write

$$\frac{1}{K_s} = \frac{1}{K_0} + \frac{1}{PV} \sum_{i=1}^{N} \frac{\delta V_i}{V_i} V_i - \frac{1}{PK_0 V} \sum_{i=1}^{N} p_{pi} V_i \tag{A3}$$

Now the two quantities $\delta V_i / V_i$ and p_{pi} have to be determined. One condition can be written down directly

$$\frac{\delta V_i}{V_i} = \frac{p_{pi}}{K_f} \tag{A4}$$

To obtain a second condition, consider State 1 in Fig. 7. Now take one pore j and reduce the pore pressure to 0. The resulting relative volume change (with respect to the unloaded case) is $\delta V_j / V_j = \theta_j P$, where θ_j is assumed to be known. Since the neighbouring inclusions are assumed to be saturated, the SCS requires $\theta_j(K,\mu)$ to be taken for $K = K_s$ and $\mu = \mu_s$, where the subscript s indicates the saturated condition. Now increase the pore pressure of the particular j-pore to P. The relative volume change of this pore is now such as if it were filled with K_s, μ_s-material and is given by P/K_s. If the relation between $\delta V_j / V_j$ and p_{pj} is linear, the two cases constructed above allow the determination of the corresponding linear equation. This equation together with (A4) can be solved for p_{pj} and $\delta V_j / V_j$

$$p_{pj} = \frac{\theta_j P}{\theta_j - \frac{1}{K_s} + \frac{1}{K_f}} \qquad \frac{\delta V_j}{V_j} = \frac{p_{pj}}{K_f} \tag{see A4}$$

If these are inserted into (A3), one finally obtains the saturated bulk modulus as a function of the apparent compressibility of dry pores

$$\frac{1}{K_s} = \frac{1}{K_0} + \frac{1}{V}\left(\frac{1}{K_f} - \frac{1}{K_0}\right) \sum_{i=1}^{N} \frac{\theta_i(K_s, \mu_s) V_i}{\theta_i(K_s, \mu_s) + \frac{1}{K_f} - \frac{1}{K_s}} \tag{A5}$$

In contrast to the Gassmann relation, (A5) accounts for possibly different pore pressures. This can be important in the case of the unrelaxed state or when considering (partly) isolated pores of different geometry. However, when considering the relaxed case of interconnected pores of different geometry one should use Gassmann's relation. In the case of inclusions of the same shape (A5) can be written

$$\frac{1}{K_s} = \frac{1}{K_0} + \left(\frac{1}{K_f} - \frac{1}{K_0}\right) \times \frac{\beta}{1 + \theta^{-1}(K_s, \mu_s) \cdot \left(\frac{1}{K_f} - \frac{1}{K_s}\right)} \tag{A6}$$

Gassmann's relation (A1), together with the self-consistent dry bulk modulus (eq. 24, where all inclusions have to be treated by the second summation) can be written in a form comparable to (A6)

$$\frac{1}{K_s} = \frac{1}{K_0} + \left(\frac{1}{K_f} - \frac{1}{K_0}\right) \times \frac{\beta}{1 + \theta^{-1}(K_d, \mu_d) \cdot \left(\frac{1}{K_f} - \frac{1}{K_0}\right)} \quad \text{(A7)}$$

It turns out that (A7) is identical with (A6) if the SCS is dropped in (A6) and in the equation for the dry bulk modulus. Mavko (1980) determined the unrelaxed bulk modulus by calculating K_d with $\theta(K_u, \mu_u)$ and inserting this into Gassmann's relation. This $\theta(K_u, \mu_u)$ agrees with that in (A6); however, instead of $1/K_s$ in the denominator of (A6), Mavko still uses $1/K_0$ as required by (A7). However, some test calculations found the difference between Mavko's approach and the self consistent form (A6) to be below 1.5% with respect to K_0. If the self consistent equation of the bulk modulus given by O'Connell and Budiansky (1977) (with Mavko's (1980) modification) is written in a form comparable to (A6) it turns out that the term $1/K_s$ is missing in the denominator.

Appendix B

The quantities occurring in eqs. 32–37 have the subscripts 1, 2, 3 which refer to filmshaped, tubular, and spheroidal inclusions, respectively. They were obtained by O'Connell and Budiansky (1977), Mavko (1980), and Wu (1966), respectively.

$$\theta_1(K,\mu,\nu) = \frac{4}{3\pi} \cdot \frac{1}{K} \cdot \frac{1-\nu^2}{1-2\nu} \cdot \frac{1}{\alpha_1} \quad \text{(B1)}$$

where α_1 is the aspect ratio of the films

$$\theta_2(K,\mu,\nu) = \frac{2}{3K}\left(\frac{2(1-\nu^2)}{1-2\nu}\frac{(2+\kappa)^2+2}{(2+\kappa)^2-2} + \frac{1}{2}(1-2\nu)\right) \quad \text{(B2)}$$

$$\theta_3(K,\mu,\nu) = K^{-1}\{1-[3(g+\phi)/2 - R(3g/2 + 5\phi/2 - 4/3)]\} \times \{1-[1+3(g+\phi)/2 - R(3g/2 + 5\phi/2)] + 0.5(3-4R)\} \times \{[g+\phi - R(g-\phi + 2\phi^2)]\}^{-1} \quad \text{(B3)}$$

where

$$\phi = \alpha_3(1-\alpha_3^2)^{-3/2}\left[\cos^{-1}\alpha_3 - \alpha_3(1-\alpha_3^2)^{1/2}\right] \quad \text{(B4)}$$

$$g = \alpha_3^2(1-\alpha_3^2)^{-1}(3\phi - 2) \quad \text{(B5)}$$

$$R = 3\mu/(3K + 4\mu) \quad \text{(B6)}$$

where α_3 = aspect ratio of spheroidal inclusions and κ: parameter describing the shape of the tubular cross-sections (see Fig. 4 or Mavko, 1980).

$$A_1(K,\mu,\nu K_f) = \frac{8}{15\pi\mu} \cdot \frac{1-\nu}{2-\nu}[(2-\nu)D + 3] \cdot \frac{1}{\alpha_1} \quad \text{(B7)}$$

where

$$D(K,\mu,K_f) = (1/K_f - 1/K_0) \cdot (\theta_1(K,\mu) + 1/K_f)^{-1},$$

$D = 1$ if $K_f = 0$.

$$A_2(K,\mu,\nu,K_f) = B_2(K,\mu,\nu) + \frac{1}{15\mu}\left(\frac{2(1-\nu)\left((2+\kappa)^2+2\right)}{(2+\kappa)^2-2} - 1 + 2\nu\right) \quad \text{(B8)}$$

$$\times\left[2(1-\nu)\left((2+\kappa)^2+2\right) - (1-2\nu)\left((2+\kappa)^2-2\right)\right]\left[-2(1-\nu)\left((2+\kappa)^2+2\right) + \mu\left((2+\kappa)^2-2\right)\right]^{-1} \times \left[\frac{1}{K} - \frac{1}{K_f} - \frac{(1-2\nu)^2}{2\mu(1+\nu)}\right]^{-1} \quad \text{(B9)}$$

$$B_2 = \left[\frac{2}{15}(1+\nu) + \frac{2}{15}(1-\nu)\frac{(2+\kappa)^2+2}{(2+\kappa)^2-2} + \frac{8}{5}(3/2-\nu)\frac{(2+\kappa)^2}{(2+\kappa)^2-2}\right]\frac{1}{\mu} \quad \text{(B10)}$$

$$A_3(K,\mu,\nu,K_f) = \frac{1}{5\mu}\left[2\left\{1 - \frac{1}{2}\left[-(1+\alpha_3^2)g/\alpha_3^2 + R\left(2 - \phi + (1+\alpha_3^2)g/\alpha_3^2\right)\right]\right\}^{-1}$$

$$
\begin{aligned}
&+\{1-\tfrac{1}{4}(3\phi+g-R(g-\phi))\}^{-1}\\
&+\big(\{1-\tfrac{1}{4}[3\phi+g-R(g-\phi)]\}\\
&\times\{B\phi(3-4R)+g-R(g+\phi-4/3)\}\\
&+2\{R(g+\phi)-g+B(1-\phi)(3-4R)\}\\
&\times\{1-\tfrac{1}{8}[9\phi+3g-R(5\phi+3g)]\\
&+\tfrac{1}{2}B\phi(3-4R)\}\\
&-2\{B(1-\phi)(3-4R)-1+\tfrac{3}{2}\phi\\
&+\tfrac{1}{2}g-\tfrac{1}{2}R(5\phi+g-4)\}\\
&\{\tfrac{1}{2}B\phi(3-4R)+\tfrac{1}{2}g-\tfrac{1}{2}R(g-\phi)\}\big)\\
&\{1-\tfrac{1}{4}[3\phi+g-R(g-\phi)]\}^{-1}\\
&\times\{R(\tfrac{3}{2}g+5/2\phi)-\tfrac{3}{2}(g+\phi)+B(3-4R)\\
&-\tfrac{1}{2}(3B-1)(3-4R)[g+\phi-R\\
&\times(g-\phi+2\phi^2)]\}^{-1}\Big] \qquad \text{(B11)}
\end{aligned}
$$

where $B=K_f/3K$ and ϕ, g, and R according to (B4), (B5) and (B6).

References

Anderson, D.L., Minster, B. and Cole, D., 1974. The effect of oriented cracks on seismic velocities. J. Geophys. Res., 79: 4011–4015.

Arndt, N.T., 1977. The separation of magmas from partially molten peridotite. Annual report of the director geophysical laboratory, Carnegie Inst. Washington, pp. 424–428.

Arzi, A.A., 1972. Experimental study of partial melting in natural rocks and subsequent creep under low stresses. Trans. Am. Geophys. Union, 53: p. 513 (abstract).

Arzi, A.A., 1974. Partial Melting in Rocks: Rheology, Kinetics and Water Diffusion. Ph.D. Thesis, Havard Univ., Cambridge, MA.

Arzi, A.A., 1978a. Fusion kinetics, water pressure, water diffusion and electrical conductivity in melting rocks, interrelated. J. Petrol., 19: 153–169.

Arzi, A.A., 1978b. Critical phenomena in the rheology of partially melted rocks. Tectonophysics, 44: 173–184.

Berckhemer, H., Auer, F. and Drisler, J., 1979. High-temperature anelasticity and elasticity of mantle peridotite. Phys. Earth. Planet. Inter., 20: 48–59.

Berckhemer, H., Kampfmann, W., Aulbach, E. and Schmeling, H., 1982a. Shear modulus and Q of forsterite and dunite near partial melting from forced oscillation experiments. Phys. Earth Planet. Inter., 29: 30–41.

Berckhemer, H., Kampfmann, W. and Aulbach, E., 1982b. Anelasticity and elasticity of mantle rocks near partial melting. In: W. Schreyer (Editor), High-Pressure Researches in Geoscience. E. Schweizerbart'sche Verlagsbuchhandlung, Stuttgart, pp. 113–132.

Biot, M.A., 1956a. Theory of propagation of elastic waves in a fluid-saturated porous solid. I. Low-frequency range. J. Acoustical Soc. Am., 28: 168–178.

Biot, M.A., 1956b. Theory of propagation of elastic waves in a fluid-saturated porous solid. II. Higher frequency range. J. Acoustical Soc. Am., 28: 179–191.

Budiansky, B., 1965. On the elastic moduli of some heterogeneous materials. J. Mech. Phys. Solids, 13: 223–227.

Budiansky, B. and O'Connell R.J., 1976. Elastic moduli of a cracked solid. Int. J. Solids Struct., 12: 81–97.

Budiansky, B. and O'Connell, R.J., 1980. Bulk dissipation in heterogeneous media. In: S. Nemat Nasser (Editor), Solid Earth Geophysics and Geotechnology. Am. Soc. Mech. Eng., New York, pp. 1–10.

Buesch, W., Schneider, G. and Mehnert, K.R., 1974. Initial melting at grain boundaries, II: Melting in rocks of granodioritic, quartzdioritic and tonalitic composition. Neues Jahrb. Mineral. Monatsh., 8: 345–370.

Bulau, J.R.., Waff, H.S. and Tyburczy, J.A., 1979. Mechanical and thermodynamic constraints on fluid distribution in partial melts. J. Geophys. Res., 84: 6102–6108.

Cooper, R.F. and Kohlstedt, D.L., 1982. Interfacial energies in the olivine-basalt system. In: S. Akimoto and M.H. Manghnani (Editors), High-pressure Research in Geophysics. Advances in Earth and Planetary Science, Center for Academic Publications, Tokyo, 12. pp. 217–228.

Eshelby, J.D., 1957. The determination of the elastic field of an ellipsoidal inclusion, and related problems. Proc. R. Soc. London Sect. A, 241: 376–396.

Gassmann, F., 1951. Ueber die Elastizität poröser Medien. Vierteljahresschr. Naturforsch. Ges. Zuerich, 96: 1–23.

Green, D.H. and Liebermann, R.C., 1976. Phase equilibria and elastic properties of a pyrolite model for the oceanic upper mantle. Tectonophysics, 32: 61–92.

Haak, V., 1980. Relations between electrical conductivity and petrological parameters of the crust and upper mantle. Geophys. Surv., 4: 57–69.

Hashin, Z., 1959. The moduli of an elastic solid containing spherical particles of another elastic material. In: W. Olszak (Editor), Proceedings of the International Union of Theoretical and Applied Mechanics Symposium on Non-homogeneity in Elasticity and Plasticity. Pergamon Press, New York, p. 463.

Hashin, Z. and Shtrikman, S., 1963. A variational approach to the theory of the elastic behaviour of multiphase materials. J. Mech. Phys. Solids, 11: 127–140.

Hill, R., 1965. A self-consistent mechanics of composite materials. J. Mech. Phys. Solids, 13: 213–222.

Johnston, D.H., Toksöz, M.N. and Timur, A., 1979. Attenuation of seismic waves in dry and saturated rocks: II. Mechanisms. Geophysics, 44: 691–711.

Kampfmann, W., 1984. Laborexperimente zum elastischen und anelastischen Verhalten hochtemperierter magmatischer Gesteine im Frequenzbereich seismischer Wellen. Dissertation, Inst. fuer Meteorologie und Geophysik, Frankfurt/Main, 37 pp.

Kingery, W.D., Bowen, H.K. and Uhlmann, D.R., 1976. Intro-

duction to Ceramics. Wiley and Sons, New York, 1032 pp.
Kjartansson, E., 1979. Attenuation due to thermal relaxation in porous rocks. Conference on seismic wave attenuation, June 25–27, 1979, Stanford Univ. Publ., Geol. Sci. XVII: 68–69 (abstract).
Korringa, J., Brown, R.J.S., Thompson, D.D. and Runge, R.J., 1979. Self-consistent imbedding and the ellipsoidal model for porous rocks. J. Geophys. Res., 84: 5591–5598.
Kushiro, I., 1977. Phase transformation in silicate melts under upper-mantle conditions. In: M.H. Manghnani and S. Akimoto (Editors), High-pressure Research. Academic Press, New York, 642 pp.
Kushiro, I., Yoder, H.S., Jr. and Mysen, B.O., 1976. Viscosities of basalt and andesite melts at high pressures. J. Geophys. Res., 81: 6351–6356.
Kuster, G.T. and Toksöz, M.N., 1974. Velocity and attenuation of seismic waves in two-phase media: Part I. Theoretical formulations. Geophysics, 39: 587–606.
Love, A.E.H., 1907. Lehrbuch der Elastizität. B.G. Teubner Verlag, Leipzig, 664 pp.
Mavko, G.M., 1980. Velocity and attenuation in partially molten rocks. J. Geophys. Res., 85: 5173–5189.
Mavko, G.M. and Nur, A., 1975. Melt squirt in the asthenosphere. J. Geophys. Res., 80: 1444–1448.
Mavko, G.M. and Nur, A., 1978. The effect of nonelliptical cracks on the compressibility of rocks. J. Geophys. Res., 83: 4459–4468.
Mavko, G., Kjartansson, E. and Winkler, K., 1979. Seismic wave attenuation in rocks. Rev. Geophys. Space Phys., 17: 1155–1164.
Mehnert, K.R., Buesch, W. and Schneider, G., 1973. Initial melting at grain boundaries of quartz and feldspar in gneisses and granulites. Neues Jahrb. Mineral. Monatsh., 4: 165–183.
Murase, T., Kushiro, I. and Fujii, T., 1977. Compressional wave velocity in partially molten peridotite. Annual Report of the Director Geophysical Laboratory, Carnegie Inst., Washington D.C., pp. 414–416.
Nowick, A.S. and Berry, B.S., 1972. Anelastic Relaxation in Crystalline Solids. Academic Press, New York, London, 677 pp.
Nur, A., 1971. Viscous phase in rocks and the low-velocity zone. J. Geophys. Res., 76: 1270–1277.
O'Connell, R.J. and Budiansky, B., 1974. Seismic velocities in dry and saturated cracked solids. J. Geophys. Res., 79: 5412–5426.
O'Connell, R.J. and Budiansky, B., 1977. Viscoelastic properties of fluid-saturated cracked solids. J. Geophys. Res., 82: 5719–5735.
Padovani, E.R., 1977. Granulite Xenoliths from Kilbourne Hole Maar, New Mexico, and their Bearing on Deep Crustal Evolution. Ph. D. Thesis, Univ. of Texas at Dallas, Richardson, 172 pp.
Reuss, A., 1929. Berechnung der Fliessgrenze von Mischkristallen auf Grund der Plastizitätsbedingung fuer Einkristalle. Z. Angew. Math. Mech., 9: 49–58.
Ringwood, A.E., 1962a. A model for the upper mantle. J. Geophys. Res., 67: 857–867.
Ringwood, A.E., 1962b. A model for the upper mantle 2. J. Geophys. Res., 67: 4473–4477.
Ringwood, A.E., 1975. Composition and Petrology of the Earth's Mantle. McGraw-Hill Book Comp., New York, 618 pp.
Scarfe, C.M., Paul, D.K. and Harris, P.G., 1972. Melting experiments on two ultramafic nodules. Neues Jarhb. Mineral. Monatsh., 10: 469–476.
Schmeling, H., 1983. Numerische Modelle ueber den Einfluss partieller Schmelze auf elastische, anelastische und elektrische Eigenschaften von Gesteinen mit Anwendung auf Labordaten und die Asthenosphäre. Dissertation, Inst. fuer Meteorologie und Geophysik, Frankfurt/Main, 268 pp.
Schmeling, H., 1984. Constraints on the degree and geometry of partial melt in the oceanic asthenosphere and beneath Iceland. Terra Cognita, 4: 255–256 (extended abstract).
Schmeling, H., 1985. Partial melt below Iceland: a combined interpretation of seismic and conductivity data. J. Geophys. Res., in press.
Schmeling, in prep.(a). Partial melt in the asthenosphere: constraints from a combined interpretation of seismic and electric data (to be submitted to J. Geophys. Res.).
Schmeling, in prep.(b). A simple model on the degree of interconnection in partially molten rocks (to be submitted to J. Geophys. Res.).
Shankland, T.J. and Waff, H.S., 1974. Conductivity in fluid-bearing rocks. J. Geophys. Res., 79: 4863–4868.
Solomon, S.C., 1972. Seismic-wave attenuation and partial melting in the upper mantle of North America. J. Geophys. Res., 77: 1483–1502.
Stocker, R.L. and Gordon, R.B., 1975. Velocity and internal friction in partial melts. J. Geophys. Res., 80: 4828–4836.
Stolper, E., Walker, D., Bradford, H.H. and Hays, J.F., 1981. Melt segregation from partially molten source regions: the importance of melt density and source region size. J. Geophys. Res., 86: 6261–6271.
Vaisnys, J.R., 1968. Propagation of acoustic waves through a system undergoing phase transformations. J. Geophys. Res., 73: 7675–7683.
Van der Molen, I. and Paterson, M.S., 1979. Experimental deformation of partially-melted granite. Contrib. Mineral. Petrol., 70: 299–318.
Voigt, W., 1928. Lehrbuch der Kristallphysik. Teubner, Leipzig, 978 pp.
Waff, H.S., 1974. Theoretical considerations of electrical conductivity in a partially molten mantle and implications for geothermometry. J. Geophys. Res., 79: 4003–4010.
Waff, H.S. and Bulau, J.R., 1979. Equilibrium fluid distribution in an ultramafic partial melt under hydrostatic stress conditions. J. Geophys. Res., 84: 6109–6114.
Walsh, J.B., 1968. Attenuation in partially melted material. J. Geophys. Res., 73: 2209–2216.
Walsh, J.B., 1969. New analysis of attenuation in partially melted rock. J. Geophys. Res., 74: 4333–4337.
Walsh, J.B. and Grosenbaugh, M.A., 1979. A new model for analyzing the effect of fractures on compressibility. J. Geophys. Res., 84: 3532–3536.
Watt, J.P., Davies, G.F. and O'Connell, R.J., 1976. The elastic properties of composite materials. Rev. Geophys. Space Phys., 14: 541–563.
Wu, T.T., 1966. The effect of inclusion shape on the elastic moduli of a two-phase material. Int. J. Solid Struct., 2: 1–8.
Wyllie, P.J., 1971. The Dynamic Earth: Textbook in Geosciences. Wiley and Sons, New York, 416 pp.
Zener, C., 1948. Elasticity and Anelasticity of Metals. The University of Chicago Press, Chicago, 170 pp.